HHS Public Access

Author manuscript

Nat Microbiol. Author manuscript; available in PMC 2020 July 20.

Published in final edited form as:

Nat Microbiol. 2020 February ; 5(2): 272–281. doi:10.1038/s41564-019-0633-0.

Select autophagy genes maintain quiescence of tissue-resident macrophages and increase susceptibility to *Listeria monocytogenes*

Ya-Ting Wang[1,2,#], **Konstantin Zaitsev**[1,3], **Qun Lu**[1,9], **Shan Li**[4], **W. Timothy Schaiff**[1,10], **Ki-Wook Kim**[5], **Lindsay Droit**[1], **Craig B. Wilen**[1,11], **Chandni Desai**[1], **Dale R. Balce**[1,10], **Robert C. Orchard**[1,12], **Anthony Orvedahl**[6], **Sunmin Park**[1], **Darren Kreamalmeyer**[1], **Scott A. Handley**[1], **John D. Pfeifer**[7], **Megan T. Baldridge**[8], **Maxim N. Artyomov**[1], **Christina L Stallings**[2,#], **Herbert W. Virgin**[1,10,#]

[1]Department of Pathology and Immunology, Washington University School of Medicine, St Louis, MO 63110, USA

[2]Department of Molecular Microbiology, Washington University School of Medicine, St. Louis, MO 63110, USA

[3]Computer Technologies Department, ITMO University, St. Petersburg, Russia

[4]Department of Cell Biology and Physiology, Washington University School of Medicine, St. Louis, MO 63110, USA

[5]Department of Pharmacology, University of Illinois College of Medicine, Chicago, IL 60612, USA

[6]Department of Pediatrics, Division of Infectious Diseases, Washington University School of Medicine, St. Louis, MO 63110, USA

[7]Lauren V. Ackerman Laboratory of Surgical Pathology, Division of Anatomic and Molecular Pathology, Department of Pathology and Immunology, Washington University Medical Center, St Louis, MO, USA

[8]Department of Medicine, Division of Infectious Diseases, Washington University School of Medicine, St. Louis, MO 63110, USA

[9]Current affiliation: Center for Life Sciences, School of Life Sciences, Yunnan University, Kunming, China

[10]Current address: Vir Biotechnology, San Francisco, CA 94158, USA

[#]Correspondence: Ya-Ting Wang wang.yating@wustl.edu; Christina Stallings stallings@wustl.edu; Herbert Virgin virgin@wustl.edu or svirgin@vir.bio.

Author contributions Y-T.W. designed the project, performed experiments, analyzed the data and wrote the manuscript. H.W.V. supervised project design and edited manuscript. C.L.S. assisted with project design and edited manuscript. Q.L., S.L., W.T.S., L.D., and C.B.W. performed experiments. K-W.K., D.R.B., R.C.O., A.O., S.P., D.K., and M.T.B. assisted with experiments or project design. C.D., and S.A.H. helped design RNAseq experiment and analyze data, K.Z. and M.N.A. analyzed RNAseq and sc-RNAseq data. J.D.P. analyzed the histology. All authors read and edited the manuscript.

Competing interests Dr. Virgin is a founder of Casma Therapeutics and PierianDx. The work reported here was not funded by either company.

[11]Current affiliation: Yale School of Medicine, New Haven, CT USA.

[12]Current affiliation: University of Texas Southwestern Medical Center, Dallas, TX USA.

Abstract

Innate and adaptive immune responses that prime myeloid cells, such as macrophages, protect against pathogens[1,2]. However, if left uncontrolled, these responses may lead to detrimental inflammation[3]. Thus macrophages, particularly those resident in tissues, must remain quiescent in between infections despite chronic stimulation by commensal microbes. The genes required for quiescence of tissue resident macrophages are not well understood. Autophagy, an evolutionarily conserved cellular process by which cytoplasmic contents are targeted for lysosomal digestion, has homeostatic functions including maintenance of protein and organelle integrity and regulation of metabolism[4]. Recent work has shown that degradative autophagy, as well as various combinations of autophagy genes, regulates immunity and inflammation[5–12]. Here, we delineate a role for the autophagy proteins Beclin 1 and FIP200, but not of other essential autophagy components ATG5, ATG16L1, or ATG7, in mediating quiescence of tissue-resident macrophages by limiting systemic interferon-γ (IFNγ) effects. Perturbation of quiescence in mice lacking Beclin 1 or FIP200 in myeloid cells results in spontaneous immune activation and resistance to *Listeria monocytogenes* infection. While antibiotic treated wild-type mice display diminished macrophage responses to inflammatory stimuli, this is not observed in mice lacking Beclin 1 in myeloid cells, establishing the dominance of this gene over effects of the bacterial microbiota. Thus, select autophagy genes, but not degradative autophagy, have a key role in maintaining immune quiescence of tissue resident macrophages, resulting in genetically programmed susceptibility to bacterial infection.

Main letter:

Listeria monocytogenes (*L. monocytogenes*) is a bacterial pathogen that replicates intracellularly in macrophages until IFNγ triggers cellular activation for effective bacterial killing[13,14]. The involvement of autophagy in this process has been largely supported by studies in cultured cells showing co-localization of autophagy markers LC3/GABARAPs and p62 to structures either induced by or containing *L. monocytogenes*[15, 16, 64] and by studies noting modestly increased *L. monocytogenes* replication in mice lacking *Atg5* in myeloid cells[17]. Moreover, *L. monocytogenes* possesses diverse strategies to avoid degradation by autophagolysosomal pathways that may circumvent the autophagy machinery to promote pathogenesis[15,18,19]. Therefore, the precise roles of autophagy in restricting *L. monocytogenes* have been challenging to reconcile. We used a genetic approach in littermate matched mice to elucidate the role for autophagy genes in resistance to *L. monocytogenes* infection. We first investigated the role for Beclin 1, a central component of the phosphatidylinositol-3-kinase (PI3K) complex that initiates autophagosome formation[20]. Compared to $Becn1^{f/f}$ (WT herein) mice, $Becn1^{f/f}Lyz2\text{-}cre^{+/-}$ ($Becn1^{myeΔ}$) mice were resistant to *L. monocytogenes* and controlled bacterial dissemination early after infection (Fig.1a, 1c). $Fip200^{myeΔ}$ mice were similarly resistant to *L. monocytogenes* (Fig. 1b, 1c). Notably, a previous report was unable to detect a difference in survival of $Fip200^{myeΔ}$ mice when infecting with a lower dose of *L. monocytogenes*, because the non-littermate WT control mice were not susceptible to that dose [64]. These

findings are distinct from the reported functions of another autophagy protein, ATG5, in controlling *L. monocytogenes* infection [17, 65]. We confirmed these earlier results as $Atg5^{myeΔ}$ mice exhibited a modest increase in *L. monocytogenes* susceptibility (Fig. 1d). In contrast, mice lacking other essential autophagy genes in myeloid cells, $Atg7^{myeΔ}$ and $Atg16l1^{myeΔ}$ showed WT-level susceptibility to infection and bacteria dissemination (Fig. 1e, 1f, Extended Data Fig. 1a). $Atg14^{myeΔ}$ mice also showed WT-level susceptibility to *L. monocytogenes*-induced lethality but harbored reduced liver bacterial burden (Fig. 1g, Extended Data Fig. 1a). The autophagy genes were all effectively excised in macrophages of these mice as measured by p62 degradation and LC3 lipidation (Extended Data Fig. 1b). These findings were particularly notable as $Atg7^{myeΔ}$ and $Atg16l1^{myeΔ}$ mice from the same facility are significantly more susceptible to *T. gondii* infection while *Atg5* is uniquely required to control *M. tuberculosis*[8,21]. Thus, resistance to *L. monocytogenes* is genetically distinct from these other infections.

Previous studies found that *L. monocytogenes* vacuolar escape and intracellular growth is independent of *Atg5* or *Becn1*[18,22], leading us to consider the alternative hypothesis that macrophages lacking Beclin 1 and FIP200 were activated *in vivo* prior to infection. We therefore analyzed naïve macrophages resident in the peritoneal cavity, as these cells provide a first line of defense against intraperitoneal *L. monocytogenes* challenge. Peritoneal macrophages from $Becn1^{myeΔ}$ mice infected *in vitro* with *L. monocytogenes* showed enhanced control of the bacterial replication, demonstrating a cell-intrinsic resistance to *L. monocytogenes* (Fig. 1h, Extended Data Fig. 1c). We found that naïve peritoneal resident macrophages, defined by surface markers as $CSF1R^{+}ICAM2^{+}CD11b^{+}$ ($ICAM2^{+}$ macrophages, Supplementary Fig. 1a), from $Becn1^{myeΔ}$ showed marked upregulation of major histocompatibility complex (MHC) class II expression (Fig. 2a), while total peritoneal cell counts, as well as absolute numbers of $ICAM2^{+}$ peritoneal macrophages and peripheral blood monocytes were unaffected (Fig. 2b, Supplementary Fig. 2b). Explanted macrophages from $Becn1^{myeΔ}$ mice expressed increased inducible nitric oxide synthase (iNOS) upon lipopolysaccharide (LPS) or IFNγ stimulation (Fig. 2c), indicating that the cells were primed *in vivo* prior to infection. Since *Lyz2-cre* disrupts genes in multiple cell lineages in addition to resident macrophages in the peritoneal cavity, including neutrophils, dendritic cells (DCs), and small peritoneal macrophages (SPM)[23,24], we next examined the effect of Beclin 1 deletions in these other cell types. We infected $Becn1^{f/f}$-*Mrp8-Cre* mice and $Becn1^{f/f}$-*CD11c-Cre* mice, which delete *Becn1* in neutrophils and in DCs/SPM, respectively. Loss of Beclin 1 from neither neutrophils nor DCs/SPM was sufficient to result in the phenotypes observed in the $Becn1^{myeΔ}$ mice (Extended Data Fig. 2), suggesting *L. monocytogenes* resistance and macrophage activation is specific to macrophage deletion of Beclin 1.

Similar to $Becn1^{myeΔ}$ mice, MHC-$II^{high}ICAM2^{+}$ macrophages were observed in naïve $Fip200^{myeΔ}$ mice but were absent in $Atg5^{myeΔ}$, $Atg7^{myeΔ}$, and $Atg16l1^{myeΔ}$ mice (Fig. 2d, 2e, Extended Data Fig. 3a–c). In $Atg14^{myeΔ}$ mice, we observed variation in macrophage MHC-II level (Extended Data Fig. 3d). However, on average, $Atg14^{myeΔ}$ mice had lower levels of MHC-$II^{high}ICAM2^{+}$ macrophages compared to $Becn1^{myeΔ}$ or $Fip200^{myeΔ}$ mice (Extended Data Fig. 3e). Global knockout of *Rubicon*, a gene mediating LC3-associated phagocytosis (LAP) and a repressor of degradative autophagy[25], had no effect on MHC-

II^{high}ICAM2^{+} macrophage in naïve mice (Fig. 2e, Extended Data Fig. 3b–c). Together, these data show that resistance to *L. monocytogenes* correlates with the level of MHC-II^{high}ICAM2^{+} macrophage observed in uninfected mice.

We next investigated whether the macrophage activation that occurs in the absence of Beclin or Fip200 expression is systemic. Blood from both *Becn1*^{myeΔ} and *Fip200*^{myeΔ} mice contained increased MHC-II^{+} monocytes (Fig. 2f, 2g). Tissue-resident macrophages from multiple tissues of *Becn1*^{myeΔ} mice expressed higher levels of MHC-II (Fig. 2h). To determine the changes in tissue pathology that were associated with the systemic macrophage activation, H&E stained sections were examined from mice that were 8–12 weeks old and observed mild inflammation in multiple tissues (Supplementary Fig 2). The lungs of *Becn1*^{myeΔ} mice showed mild, patchy bronchiolitis with perivascular lymphoid aggregates without associated bronchiectasis, interstitial fibrosis, acute lung injury, or vasculitis. Very mild, widely spaced periportal aggregates of chronic inflammatory cells were present in the liver of these mice, without associated fibrosis or necrosis. The kidneys showed very mild patchy interstitial chronic inflammation without associated fibrosis or vasculitis, or overt evidence of glomerulitis or glomerulosclerosis in the *Becn1*^{myeΔ} mice. The spleens of *Becn1*^{myeΔ} mice showed increased extramedullary hematopoiesis.

To better define the activation state of macrophages prior to infection, we performed RNAseq on ICAM2^{+} macrophages from the peritoneum of WT and *Becn1*^{myeΔ} mice. Genes whose expression was elevated in the absence of Beclin 1 included interferon-stimulated genes (ISGs) and inflammatory cytokines (Fig. 2i, Extended Data Fig. 4a, and Supplementary Table 1). Gene set enrichment analysis demonstrated significant upregulation of IFNγ and IFNαβ responsive genes (Fig. 2j, Extended Data Fig. 4b, Supplementary Fig. 3). qRT-PCR validated findings from RNAseq (Fig. 2k, Extended Data Fig. 4c). Upregulation of inflammatory cytokines *Cxcl9*, *Cxcl10*, and *Ccl5* also suggested that Beclin 1 deficient macrophages were activated in naïve mice (Fig. 2k). Similar upregulation of IFN response genes and inflammatory cytokines were observed in FIP200-deficient macrophages (Supplementary Fig. 4).

To understand the cellular events that associated with proinflammatory macrophage activation, we analyzed DNA damage responses, as accumulating evidence highlights direct links between DNA damage response and innate immune response signaling that lead to inflammatory cytokine production[26–29]. However, we did not observe changes in the DNA damage response in resting or Bleomycin treated Beclin 1-deficient macrophages compared to WT cells (Extended Data Fig. 5a). Since peritoneal resident macrophages are maintained in the peritoneal cavity through self-renewal, we wondered if macrophage activation was associated with a replication defect in Beclin 1 deficient macrophages. Peritoneal resident ICAM2+ macrophages from both WT and *Becn1*^{myeΔ} mice undergo slow basal *in situ* proliferation (Extended Data Fig. 5b). This is consistent with previous reports of low levels of BrdU+ proliferating macrophages in steady-state[23]. To induce rapid local expansion of peritoneal resident macrophages, we injected mice with IL-4 complex (IL-4c)[30]. In WT mice, we observed increased proliferation and accumulation of ICAM2^{+} macrophages upon IL-4c injection (Extended Data Fig. 5c). In contrast, ICAM2^{+} macrophages from *Becn1*^{myeΔ} mice displayed limited replication in response to IL-4c, although they still expressed

alternative activation marker RELMα (Extended Data Fig. 5c). These results suggested that Beclin 1 regulates proliferation but not polarization of resident macrophages in response to IL-4c, which may link to its function in controlling macrophage activation.

Given our observations that Beclin 1 influences peritoneal macrophage activation state and proliferation, we performed a more global analysis of the peritoneal cell populations that rely on Beclin 1 expression in myeloid cells using single-cell transcriptomic analysis (sc-RNAseq). Cells from both *Becn1*^{myeΔ} and WT mice were partitioned into 20 clusters (C1–C20, Supplementary Fig. 5). Myeloid clusters (C1–C10) demonstrated a core transcriptional program of *Csf1r* (Fig. 3a–b). In WT mice, C1 and C2 represented tissue-resident peritoneal macrophages with high levels of *Adgre1*, *Timd4* and *Gata6* expression[31–33] (Fig. 3b). We identified a macrophage subpopulation (C4) bridging monocytes (C9) and small peritoneal macrophages (C8) with tissue-resident macrophages (C1/C2) (Fig. 3a). Reduced expression of genes that defined the core tissue-resident feature (*Adgre1*, *Gata6*, *Timd4*) and elevated *Ccr2* levels implied a monocyte origin of C4 cells (Fig 3b). This is in agreement with the idea that intermediates between newly arrived monocytes and fully mature tissue-resident macrophages are present in the peritoneum[34].

Cells from *Becn1*^{myeΔ} mice exhibited distinct clustering with the major populations shifted away from the C1/C2 clusters present in WT mice to C3/C4 and two distinct clusters C5/C6 (Fig. 3a). *Becn1*^{myeΔ} ICAM2^{+} macrophages exhibited elevated expression of IFN pathway genes (Fig. 3c), confirming RNAseq analysis (Fig. 2i–j). The accumulation of intermediate C4 and appearance of C6, macrophages with low *Adgre1*, *Gata6*, and *Timd4* expression, suggested a role for Beclin 1 in maintaining expression of tissue-specific genes in these macrophages (Fig. 3a–b). C4 and C6 macrophages exhibited varying transcriptional patterns intermediate between tissue-resident macrophages and monocyte-derived cells observed in WT mice (Supplementary Fig. 5d). In addition, compared to WT, *Becn1*^{myeΔ} mice showed accumulation of *Ccr2*$^{+}$*Itgax*$^{−}$ monocytes in C9 (Fig. 3a–b). Consistent with these findings, flow cytometry analysis identified an increase of CSF1R^{+}MHC-II^{+}ICAM2$^{−}$ cells in *Becn1*^{myeΔ} mice, which included an accumulation of CD226$^{−}$ monocytes-like cells and DCs, whereas the CD226^{+} small peritoneal macrophage population was unaltered (Fig. 3d). Together these data indicated that the differentiation and activation state of resident peritoneal macrophages depends on expression of Beclin 1.

We next examined the effects of myeloid cell deficiency of Beclin 1 on other peritoneal cells. B cells were grouped into *Zbtb32*$^{+}$ B1 cells (C11, C12, and C14)[35], *Ccr7*$^{+}$ *Sell*$^{+}$ B2 cells (C13), and *Mki67*$^{+}$ proliferating B cells (C15) (Fig. 3e, Extended Data Fig. 6a). Reduced B cell numbers were observed in *Becn1*^{myeΔ} mice (Extended Data Fig. 6a). Flow cytometry confirmed that total B cells and B1 cells were reduced in *Becn1*^{myeΔ} mice (Fig. 3f–g, Extended Data Fig. 6b), which correlated with decreased macrophage expression of *Cxcl13* (Fig. 3b, Supplementary Fig. 5)[33,36]. T cells were divided into naïve (C16) and activated T cells (C17) by *Sell* (CD62L), *Cd44* and *Ccr7* levels (Fig. 3h, Extended Data Fig. 6c), with naive T cells reduced in *Becn1*^{myeΔ} mice (Fig. 3i, Extended Data Fig. 6d). Notably, *Becn1*^{myeΔ} mice showed increased *Ifng* expression in T cells and NK cells (Fig. 3j). *Ifng* transcription was mainly found in activated T cells (Fig. 3k, Extended Data Fig. 6e). These data show that there are considerable effects of myeloid cell deficiency of Beclin 1 on

bystander immune cells such that immune homeostasis is substantially disrupted. Perturbed homeostasis with reduced B1 cells and activation of T cells were also observed in *Fip200*^{myeΔ} mice (Supplementary Fig. 6).

We next investigated the immune mechanism responsible for the disruption in the structure and function of the immune system observed in the peritoneum of *Becn1*^{myeΔ} mice. Although previous reports have linked autophagy deficiency to inflammasome activation[6,37–39], introduction of *Casp1/11* deficiency did not influence MHC-II levels or *L. monocytogenes* resistance in Beclin 1-deficient macrophages (Fig. 4a, 4d, Extended Data Fig. 7a–c). Based on the elevated IFN pathways from RNAseq and sc-RNAseq results, we tested the hypothesis that proinflammatory macrophage activation in uninfected mice lacking myeloid Beclin 1 is driven by IFNγ. Although autophagy inhibits type I IFN production and type I IFN pathway is enriched due to overlapping gene sets with IFNγ pathway, this pathway is detrimental during *L. monocytogenes* infections[40–43]. Introduction of IFNγ receptor deficiency (*Ifngr*^{Δ}) abolished MHC-II^{high}ICAM2^{+} macrophages in *Becn1*^{myeΔ}*Ifngr*^{Δ} mice, indicating an essential role for IFNγ in the activation of macrophages in *Becn1*^{myeΔ} mice (Fig. 4a–b). *Ifngr*^{Δ} also restored systemic immune homeostasis, diminishing MHC-II^{+} monocyte numbers (Fig. 4c) and rescuing the abnormal phenotypes of B and T cell populations, monocyte accumulation and neutrophil infiltration observed in the peritoneum of *Becn1*^{myeΔ} mice (Extended Data Fig. 8).

Given the role of T cell-derived IFNγ in virus-induced systemic inflammation[10], and increased *Ifng*$^{+}$ T cells revealed by sc-RNAseq, we assessed the involvement of T cells in eliciting proinflammatory macrophages in *Becn1*^{myeΔ} mice. Elimination of T and B cells in *Rag1*^{Δ} mice diminished but did not eliminate macrophage activation (Fig. 4a, 4d, Extended Data Fig. 7a–b). Compared to age- and sex-matched *Becn1*^{myeΔ} mice *Becn1*^{myeΔ}*Rag1*^{Δ} mice had fewer MHC-II high macrophages (*Becn1*^{myeΔ}B6/J, 73.6%±8.4; *Becn1*^{myeΔ}*Rag1*^{Δ}, 27.2%±3.7, $P<0.0001$). These data suggested that, while IFNγ from T cells in the *Becn1*^{myeΔ} mice influenced macrophages, additional IFNγ from innate immune cells can also drive macrophage activation, albeit at a lower level, in the setting of Beclin 1-deficiency. Deletion of either the IFNγ receptor (*Becn1*^{myeΔ}*Ifngr*^{Δ}) or adaptive immune cells (*Becn1*^{myeΔ}*Rag1*^{Δ}) ablated the protective effect of *Becn1* myeloid deletion against *L. monocytogenes* (Fig. 4e, 4g, Extended Data Fig. 7d). Neutralizing IFNγ also diminished the enhanced resistance to *L. monocytogenes* in *Fip200*^{myeΔ} mice (Fig. 4f). These data demonstrate that IFNγ is required for protection from *L. monocytogenes* challenge in *Becn1*^{myeΔ} mice and there is a critical role for activated macrophages and bystander lymphocytes in this process.

Unlike adult mice, neonatal *Becn1*^{myeΔ} mice lacked signs of macrophage activation on postnatal days 14~16 (Fig. 4h). Gut microbiota was reported to mediate ISG expression in the intestinal tissue of ATG16L1 deficient mice[44]. Since a major early life event is the acquisition and establishment of the microbiota and commensal microbes set the level of immune activation of immune cells in naïve mice[45–47], we considered the possibility that the activation of tissue-resident macrophages in adult mice is influenced by the microbiota. As such, we confirmed prior studies showing that macrophages from antibiotic-treated WT mice exhibited reduced responses to IFNγ and LPS *ex vivo* (Fig. 4i)[45]. In contrast to WT

mice, antibiotic treatment did not diminish the responsiveness of explanted macrophages from *Becn1*^{myeΔ} mice to either IFNγ or LPS (Fig. 4i). Consistent with these findings, antibiotic-mediated depletion of commensal bacteria had no effect on the proinflammatory activation of peritoneal resident macrophages in *Becn1*^{myeΔ} mice (Fig. 4j, Extended Data Fig. 9a). The lack of an effect of antibiotics in *Becn1*^{myeΔ} mice was not due to inefficient microbial depletion since, as previously reported, antibiotics diminished bacterial population based on quantifying 16S copies (Extended Data Fig. 9b) and reduced CD226^{+} small peritoneal macrophages in both *Becn1*^{myeΔ} and WT mice (Fig. 4k, Extended Data Fig. 9c)[48]. Importantly, deletion of the IFNγ receptor partially enabled the effects of the antibiotics on the activation of explanted macrophages in antibiotic-treated *Becn1*^{myeΔ} mice (Fig. 4l). This indicates that the peritoneal resident macrophages are chronically stimulated by the bacterial microbiota to maintain basal responsiveness. Beclin 1 deletion increased the activation of these cells, presenting a dominate effect over the effects of the bacterial microbiota, in a manner that requires IFNγ. Although transient depletion of microbiota was not able to restore the quiescent macrophages in *Becn1*^{myeΔ} mice, we cannot rule out that the microbiota may play a role during development of the activated macrophages in these mice.

We have demonstrated herein a role for Beclin 1 and FIP200 in maintaining immune quiescence of tissue resident macrophages. Loss of these genes in myeloid cells of uninfected mice perturbs the homeostasis of cell-cell communication between lymphoid and myeloid cells, prompting the production of IFNγ by activated T cells in a feed-forward manner leading to activation of the immune system and altered macrophage differentiation. There were significant physiological consequences of immune quiescence regulation. On the one hand, immune activation associated with myeloid deficiency in Beclin 1 or FIP200 accelerated clearance of intracellular bacteria, while on the other hand the regulation of the basal activation state of macrophages by antibiotics was ablated. In addition, peritoneal macrophage proliferation in response to IL-4 was diminished. *Becn1*^{myeΔ} mice exhibited increased activation of multiple tissue resident macrophages and blood monocytes. Therefore, the role of Beclin 1 in immune quiescence is systemic, but the implications of this appear to be pathogen or tissue specific. For example, in contrast to our data with *L. monocytogenes*, *Becn1*^{myeΔ} mice did not exhibit enhanced resistance to pulmonary influenza infection (Extended Data Fig. 10). Resistance to influenza is observed as a result of myeloid deficiency of multiple other autophagy genes, including *Atg5* and *Atg7*, which did not increase resistance to *L. monocytogenes*[9]. Thus, in contrast to other situations where degradative autophagy, LAP, or secretion of lysosomal contents regulates aspects of immunity system[10,11,49–52], we found that Beclin 1 and FIP200 play a distinct key role in specific aspect of immune homeostasis. This function was independent of the ubiquitin-like LC3-conjugation machinery required for selective autophagy and efficient generation and closure of the mammalian autophagosome[53]. Therefore, the role of Beclin 1 and FIP200 in maintaining immune quiescence that we observed here is distinct from a previous report where older mice (>52 weeks) develop lupus-like inflammatory disease due to the deficiency in clearing dead cells that dependent on LAP[11]. While germ line deletion of most *Atg* genes are neonatal lethal, *Becn1*$^{-/-}$ and *Fip200*$^{-/-}$ homozygotes are embryonic lethal at E7.5–15.5[54]. This further supports that Beclin 1 and FIP200 have functions outside of canonical autophagy that are critical for development or homeostasis. These differential requirements

for specific autophagy genes in different cell types and in responding to different stimuli, indicate that genes in this evolutionarily-conserved system have multiple independent roles in inhibiting inflammation. These data further suggest that the host uses cellular stress response genes to render cells of the myeloid lineage quiescent in the basal state. The price paid for this quiescence, which likely evolved to restrict autoimmunity and to limit detrimental immune and inflammatory responses[11,55], is genetically programmed susceptibility to lethal bacterial infection.

Methods:

Mice

Atg5$^{f/f}$ and *Atg5*$^{f/f}$-*Lyz2cre*$^{+/-}$ mice were generated as described previously in an enhanced barrier facility[17,56]. *Becn1*$^{f/f}$- *Lyz2cre*$^{+/-}$[57], *Fip200*$^{f/f}$- *Lyz2cre*$^{+/-}$[58], *Atg7*$^{f/f}$-*Lyz2cre*$^{+/-}$[51], and *Atg16l1*$^{f/f}$- *Lyz2cre*$^{+/-}$ [59] were generated in the same way as *Atg5*$^{f/f}$- *Lyz2cre*$^{+/-}$. *Becn1*$^{f/f}$- *CD11c-cre*$^{+/-}$, and *Becn1*$^{f/f}$- *Mrp8-cre*$^{+/-}$ were generated by breeding *Becn1*$^{f/f}$ to *CD11c- cre*$^{+/-}$ (#007567) and *Mrp8-cre*$^{+/-}$ (#021614) from the Jackson Laboratory. *Rag1*$^{-/-}$ (#002216), *Ifngr*$^{-/-}$ (#003288), and *Casp1/11*$^{-/-}$ (#016621) mice were from the Jackson Laboratory. *Rubicon*$^{-/-}$ knockout mice were kindly provided by Doug Green and Jennifer Martinez[25]. All mice used for experimental procedures were backcrossed in house to B6/J except for *Rubicon*$^{-/-}$ mice. 8–12 weeks of age and sex-matched littermates were used unless specified otherwise and were subject to randomization. Statistical consideration was not used to determine mouse sample sizes. Mice were housed and bred at Washington University in St. Louis in specific pathogen-free conditions in accordance with federal and university guidelines, and protocols were approved by the Animal Studies Committee of Washington University.

L. monocytogenes and Influenza virus infection

L. monocytogenes wild type strain EGD was used for this study. *Listeria* glycerol stocks were stored at −80 °C, and thawed and diluted into PBS for intraperitoneal (i.p.) injection into mice. To determine tissue burden, spleens and livers were homogenized in 1 ml PBS containing 0.05% Triton X-100 and serial dilutions were plated on brain heart infusion agar plates. *Listeria* CFU were counted after overnight growth at 37°C. The H1N1 Influenza virus A strains used was A/Puerto Rico/8/1934 (PR8). Six- to eight-week-old mice were infected with 250 TCID50 (50% tissue culture infectious dose) of PR8 intranasally, weight loss and morbidity and mortality were monitored.

Ex vivo L. monocytogenes bactericidal essay

Protocol was adapted from previous reports[60]. Briefly, peritoneal cells from naïve mice were plated in DMEM + 10% heat-inactivated fetal bovine serum (FBS) supplemented with non-essential amino acid, sodium pyruvate, HEPES, and 50 U/ml penicillin and 50 μg ml^{-1} streptomycin in 96 well plates (Costar, Corning, NY) at 1 × 10^5 cells per well and allow to adhere at 37°C. Non-adherent cells were removed by washing three times with warm antibiotic-free media and 5 × 10^5 *Listeria* were put into each well. Plates were centrifuged at 600 × g for 5 min at room temperature to synchronize the infection of cells and then were incubated at 37°C for 15 min (time 0). After an additional 15 minutes at 37°C, media was

again aspirated and changed to media containing 5 μg ml^{-1} gentamicin (GIBCO). At designated time points post-infection, cells were washed five times in warm PBS, and then lysed with cold sterile deionized water with 0.1% Triton X-100. Serial dilutions of lysates were plated on BHI-agar plates to enumerate CFU.

Treatment of mice with IL-4c complexes, BrdU labeling and intracellular staining

IL-4c complexes were prepared fresh as described[30,61]. IL-4 (PeproTech) and anti-IL-4 (clone 11B11; BioXCell BE0045) were combined in a 1:5 ratio by mass using mg ml^{-1} cytokine and 5 mg ml^{-1} antibody. Complexes were incubated for ~2 min at room temperature, diluted in PBS and injected i.p. in 300uL volume per mouse. Control injections were 0.1% BSA diluted in 1× DPBS. Mice received injections on day 0 and day 2, followed by sacrifice on day 4. BrdU labeling was done according the manufacture protocol (BD 552598). BrdU was injected i.p. into mice 3 hours before harvesting the cells. For RELMα staining, the cells were first stained for surface markers and then permeabilized using Fixation/Permeabilization Solution Kit (BD 554714). Following blocking with mouse and rabbit serum, samples were stained with RELMα antibody (PeproTech 500-P214) for 1 h at room temperature and subsequently with secondary antibody for 20 min at room temperature before flow cytometry analysis.

Peritoneal cell isolation, tissue leukocyte collection, and flow cytometric analysis

Peritoneal cells were harvested after a 5-ml injection of DMEM containing 2 mM EDTA and 2% FBS into the peritoneal space. Peritoneal cells of pups were harvested by 500 μl injection. Total peritoneal leukocytes were counted using an automated cell counter (Invitrogen). Blood was collected by submandibular bleeding into EDTA or lithium heparin tubes. Lungs, liver, and spleen were excised, placed in DMEM containing 10% FBS, minced finely, and digested at 37 °C for an hour with mechanical disruption with a stir bar and enzymatic digestion. Lung was digested with Liberase Blendzyme III (Roche), hyaluronidase (Sigma-Aldrich), and DNase I (Sigma); spleen with collagenase B (Roche) and DNase I (EMD); liver, collagenase D and DNase I as described. Isolations of small intestinal lamina propria cells were performed as described[9,61]. Cells were treated with ACK buffer to remove red blood cells and were passed through a 70 μm cell strainer to generate single cell suspension.

Cells were suspended in PBS with 2mM EDTA, 0.1% sodium azide, and 3% FBS. Peritoneal cells were blocked with anti-FcγRII/III (biolegend 101302) and labeled with specific antibodies against CSF1R (eBioscience 46–1152-80), ICAM2 (Biolegend 105606), F4/80 (eBioscience 25–4801-82), CD226 (biolegend 128805), Ly-6G (BioLegend 127624), I-A/I-E (BioLegend 107631), CD11b (BioLegend 101237), TCRb (eBioscience 11–5961-85), CD19 (BD 552854), CD5 (BD 553022), CD62L (BioLegend 104432), CD44 (BioLegend 103012). Total cell number was multiplied by the percentage of specific cell type in total single cells, as analyzed by flow cytometry.

Gating of tissue/blood cell populations was as described[61]. Briefly, blood monocytes were gated as $CD45^+Ly6G^-Ly6C^+CD11b^+$. Lung alveolar macrophages were gated as $CD45^+$Siglec-F^+CD11c^+. Liver Kupffer cells were gated as $CD45^+F4/80^+$ $CD11b^{lo}Ly6C^-$.

Spleen red pulp macrophages were gated as F4/80^{hi}CD11b^{lo} CD11c^{lo} and negative or low for other markers. Small intestinal lamina propria macrophages were gated as CD45^{+}F4/80^{+}CD64^{+} Ly6C^{-} MHC-II^{+} (for isotype control sample: CD45^{+}F4/80^{+}CD64^{+}Ly6C^{-}). Flow cytometric analysis was performed on an LSRFortessa (BD Biosciences) and data analyzed with FlowJo software (Tree Star Inc.).

Peritoneal macrophage western blot, immunofluorescent, and *ex vivo* stimulation

Adherent macrophages were lysed using RIPA buffer (Sigma), and then diluted in 2X Laemmli buffer, resolved using 4–20% polyacrylamide gels (BioRad) transferred to PVDF membrane (BioRad) and detected with the following antibodies: LC3b (Sigma L7543), p62/SQSTM1 (Sigma P0067), and GAPDH-HRP (sigma G9295) or secondary goat-anti-Rabbit-HRP (Jackson 111–035-144). HRP was detected using ECL (Biorad). For immunofluorescence (IF), adherent macrophages were stimulated with 1 μg/mL bleomycin or unstimulated. Cells were fixed and permeabilized before staining with antibodies against γ-H2AX (clone JBW301, Millipore) and p62/SQSTM1 (GP62-C, Progen). For analyzing iNOS, adherent macrophages were stimulated with 20 unit/mL recombinant IFN-γ (R&D Systems) and 10ng/mL LPS (Sigma), After stimulation, media was removed and replaced with cold PBS with 2 mM EDTA incubated on ice for 10 min to detach the cells. Cells were first stained for live cells (Live/Dead Fixable Aqua, Invitrogen) and surface staining with antibodies. Following by fixation and permeabilization using BD Cytofix/Cytoperm (BD Biosciences), cells were stained for iNOS (eBioscience 17–5920-82) and analyzed with flow cytometry.

RNA Isolation, RNAseq, and qRT-PCR

For RNAseq, peritoneal macrophage from naïve mice were purified by sorting on AriaII (BD Biosciences) with >95% purity. RNA was isolated from cells with an RNeasy mini-kit (QIAGEN) and from peritoneal cells in accordance with the manufacturer's instructions. an mRNA Illumina sequencing library was generated and run on an Illumina HiSeq as previously described[9,10]. Each group contain n=4 samples, and each sample contains RNA extracted from 3 sorted biological replicates. DESeq2 was used for differential gene expression analysis[62] which was used as ranked list in pre-ranked GSEA analysis to identify pathway enrichments as previously described[10]. For qRT-PCR, RNA was extracted from sort purified or adherent macrophages using RNeasy mini kit (Qiagen) followed by cDNA synthesis using ImProm II (Promega). Real time qPCR using Taqman based assays (IDT) and copy numbers were determined using a standard curve. Actb (Mm.PT.58.33540333) H2-Eb1 (Mm.PT.58.5936748); H2-Ab1 (Mm.PT.58.42625719.g); Ciita (Mm.PT.58.41742531); STAT1 (Mm.PT.58.23792152); IRF1 (Mm.PT.58.33516776); Cxcl9 (Mm.PT.58.5726745); Cxcl10 (Mm.PT.58.43575827); CCL-5 (Mm.PT.58.43548565); GBP4 (Mm.PT.58.13413468); Gbp8 (Mm.PT.58.33178892); SOCS1 (Mm.PT.58.11527306.g); igf1 (Mm.PT.58.32726889); Emr1 (Mm.PT.58.11087779). Genes of interest were normalized to β-actin copy numbers.

Single-cell RNAseq data generation

Peritoneal cells were partitioned into nanoliter-scale Gel Bead-In-EMulsions (GEMs) to achieve single-cell resolution for a maximum of 10,000 individual cells per sample.

Utilizing the v2 Chromium Single Cell 3' Library Kit and Chromium instrument (10x Genomics), poly-adenylated mRNA from an individual cell was tagged with a unique 16 basepair 10x barcode and 10 basepair Unique Molecular Identifier. Full length cDNA was amplified to generate sufficient mass for library construction. Enzymatic fragmentation and size selection were used to optimize the cDNA amplicon size (~400 basepair) for the library. The final library was sequence-ready and contained four unique sample indexes. The concentration of the 10x single cell library was determined through qPCR (Kapa Biosystems). The libraries were normalized, pooled, and sequenced with a custom recipe (26–8-98) on the HiSeq4000 platform (Illumina). Two single-cell libraries were sequenced across an entire HiSeq4000 flow cell targeting ~90,000 reads per cell.

Alignment, barcode assignment and unique molecular identifier (UMI) counting

The Cell Ranger Single-Cell Software Suite (version 2.0.2) (https://support.10xgenomics.com/single-cell-gene-expression/software/pipelines/latest/what-is-cell-ranger) was used to perform sample demultiplexing, barcode processing, and single-cell 3' counting. Cellranger mkfastq was used to demultiplex raw base call files from the HiSeq4000 sequencer into sample-specific fastq files. Files was demultiplexed with 98%+ perfect barcode match, and 72%+ q30 reads. Subsequently, fastq files for each sample were processed with cellranger to align reads to mm10 genome.

Preprocessing analysis with Seurat package

For the analysis, the Seurat package (version 2.3.4) (Butler and Satija, 2017) was used. Cell Ranger filtered genes by barcode expression matrices were used as analysis inputs. Samples were pooled together using the AddSample function. Expression measurements for each cell were normalized by total expression and then scaled to 10,000, after that log normalization was performed.

Dimensionality reduction and clustering

The most variable genes were detected using FindVariableGenes function. PCA was run only using these genes. Cells are represented with t-SNE (t-distributed Stochastic Neighbor Embedding) plots. We applied RunTSNE function to normalized data, using first 10 PCA components. For clustering, we used function FindClusters that implements SNN (shared nearest neighbor) modularity optimization-based clustering algorithm on 10 PCA components with a resolution of 0.8. Twenty clusters were detected, one of which contained poorly covered cells (lower number of UMIs and detected genes); this cluster was excluded from further analysis.

Heatmaps

All heatmaps were generated using Phantasus web service (https://artyomovlab.wustl.edu/phantasus/). For bulk RNA-seq counts were log2 quantile normalized prior to heatmap generation. For single-cell RNA-seq scaled expression values for every gene were averaged per cluster and then log2 normalized prior to heatmap generation.

Single-cell RNA-seq differential expression

To obtain differential expression between clusters and Ifng expression between conditions in T cells, a MAST test was performed and P value adjustment was performed using a Bonferroni correction (Finak et al., 2015).

Antibiotic treatment of mice

Adult C57BL/6 mice were treated orally with a combination of broad-spectrum antibiotics, as previously described[63]: vancomycin (0.5 g/liter; Sigma-Aldrich), neomycin (1 g/L; Sigma-Aldrich), ampicillin (1 g/L; Sigma-Aldrich), and metronidazole (1 g/L; MP Biomedicals) dissolved in grape Kool-Aid (20 g/L; Kraft Foods). This solution was substituted for drinking water for 2 weeks before euthanasia and cell analysis; control mice received the grape Kool-Aid without antibiotics.

Quantification and Statistical analysis

Data were analyzed with Prism 7 software (GraphPad Software, San Diego, CA). In all graphs, four asterisks indicate a P value of <0.0001, three asterisks indicate a P<0.001, two asterisks indicate a P<0.01, one asterisk indicates a P<0.05, and ns indicates not significant (P >0.05) as determined by Mann-Whitney test, Gehan-Breslow-Wilcoxon test, 2way ANOVA with Tukey's multiple-comparison test or Kruskal-Wallis test or Sidak's multiple comparisons test, as specified in the figure legends.

Data Availability

The data that support the findings of this study are available from the corresponding author upon request. RNA-seq data are available at the European Nucleotide Archive (PRJEB29191). Single-cell RNAseq data is available on GEO database (GSE121521).

Extended Data

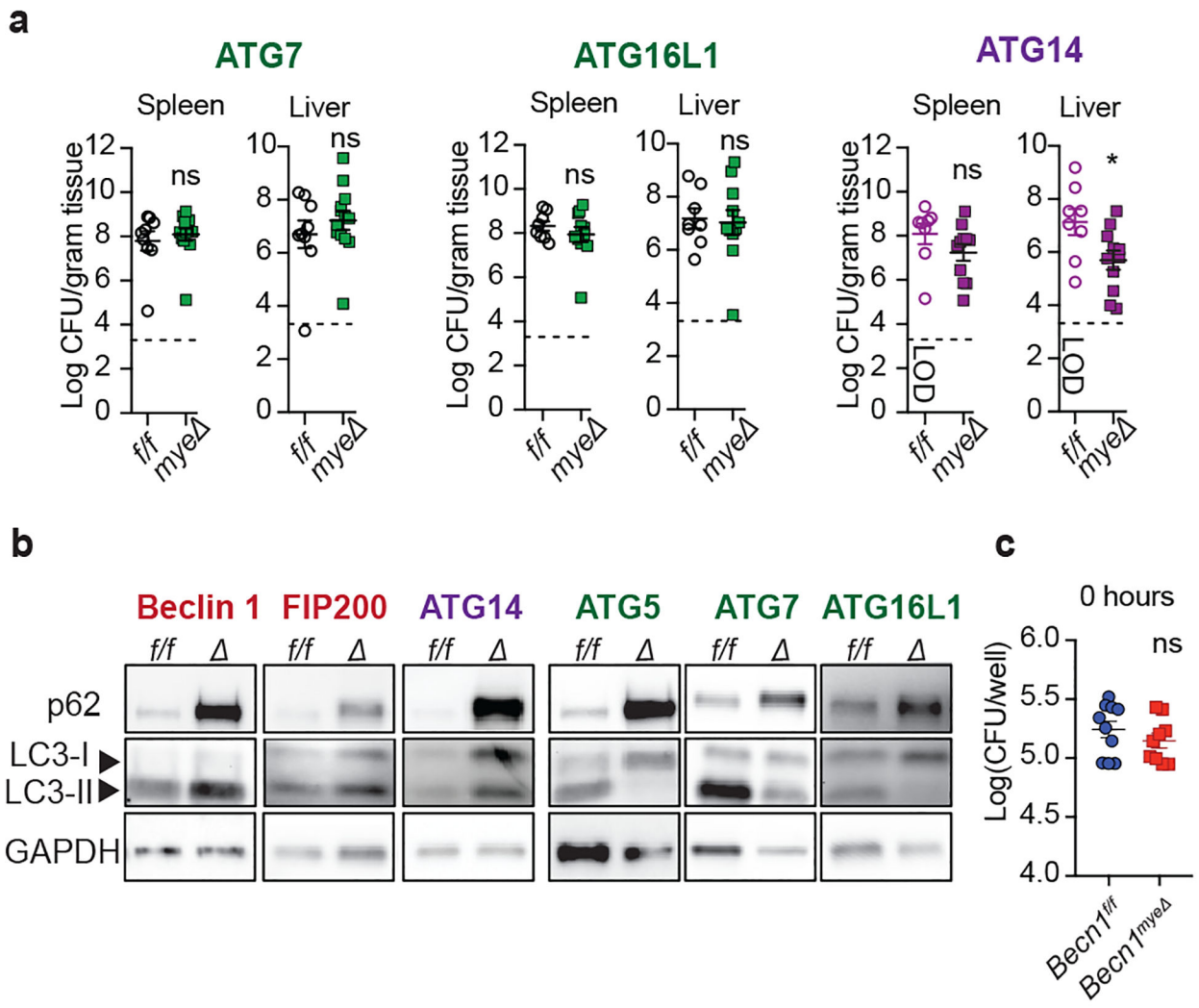

Extended Data Fig. 1. Mice with deficiencies of certain autophagy genes in myeloids cells display enhanced resistance to *L. monocytogenes*.

a, *L. monocytogenes* CFU in spleen or liver 3 days after infection of mice harboring myeloid deficiency (*myeΔ)* in multiple autophagy genes (data pooled from 2 experiments, $Atg7^{f/f}$, n=9; $Atg7^{myeΔ}$, n=13; $Atg16l1^{f/f}$, n=8; $Atg16l1^{myeΔ}$, n=10; $Atg14^{f/f}$, n=8; $Atg14^{myeΔ}$, n=11 mice; mean ± SEM; P by 2-tailed t test).

b, Western blot analysis of p62, LC3 and GAPDH in peritoneal macrophages from naïve mice (Representative of n≥3 replicates).

c, *Ex vivo* phagocytosis activity of peritoneal macrophages at 0 hour (data pooled from 2 experiments, $Becn1^{f/f}$, n=12; $Becn1^{myeΔ}$, n=11; mean ± SEM; *ns*=not significant by 2-tailed t test)

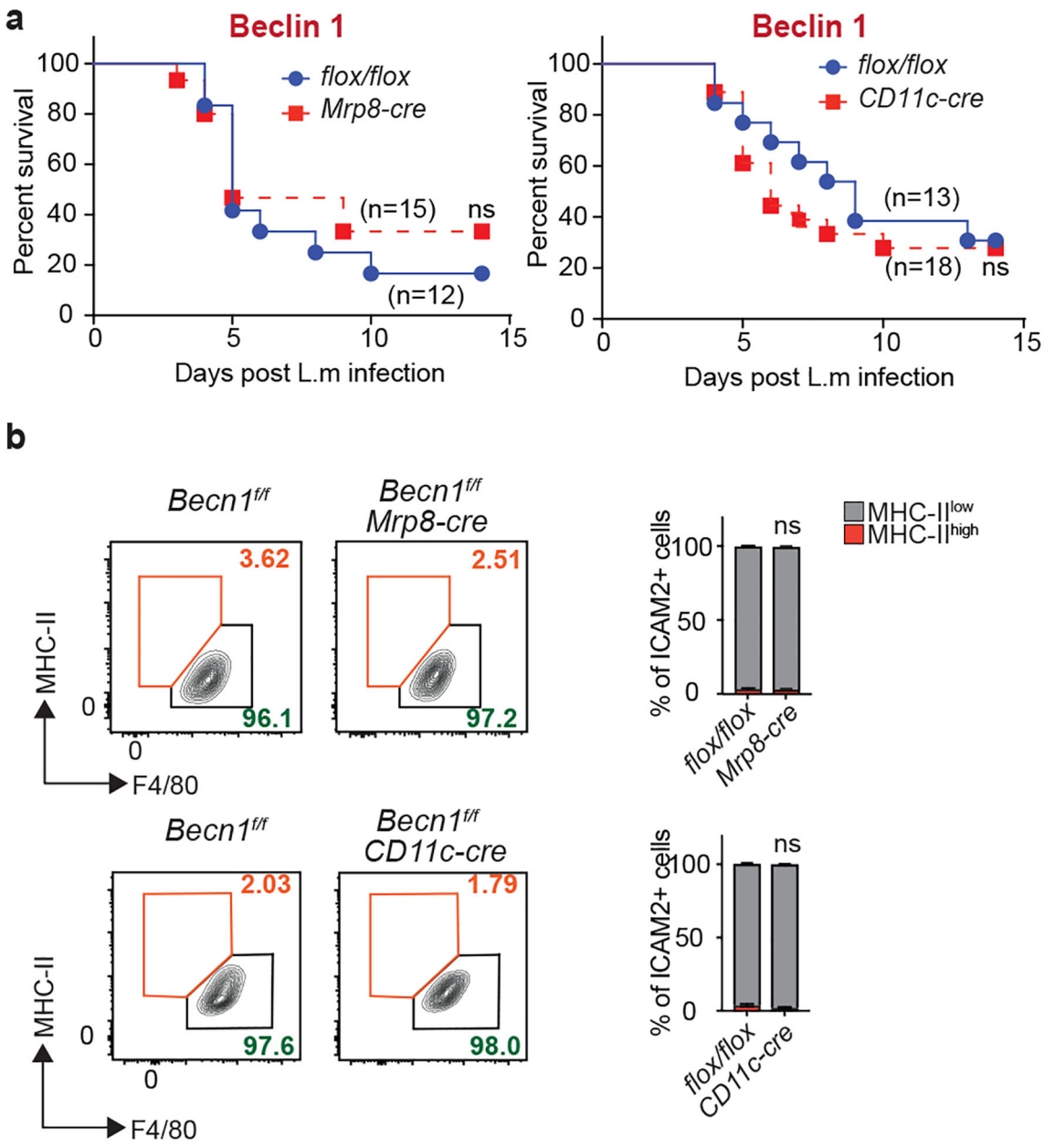

Extended Data Fig. 2. Mice with Beclin 1 deletion in DCs or neutrophils do not display *L. monocytogenes* resistance or macrophage activation phenotype.

a, Survival of mice harboring Beclin 1 deletion in $CD11c^+$ and $MRP8^+$ cells vs littermate controls, after i.p. inoculation with $4\sim5\times10^5$ CFUs of *L. monocytogenes* (Data pooled from 3–4 experiments; not significantly different by Log-rank Mantel-Cox test).

b, Flow cytometry of $ICAM2^+$ macrophage subsets in peritoneum of adult naïve mice (Data represents 2 experiments, *Becn1*$^{f/f}$, n=3 vs *Becn1*$^{f/f}$*-Mrp8-cre*, n=3; *Becn1*$^{f/f}$, n=5 vs *Becn1*$^{f/f}$*-CD11c-cre*, n=4; mean ± SEM; not significant by 2way ANOVA Sidak's multiple comparisons).

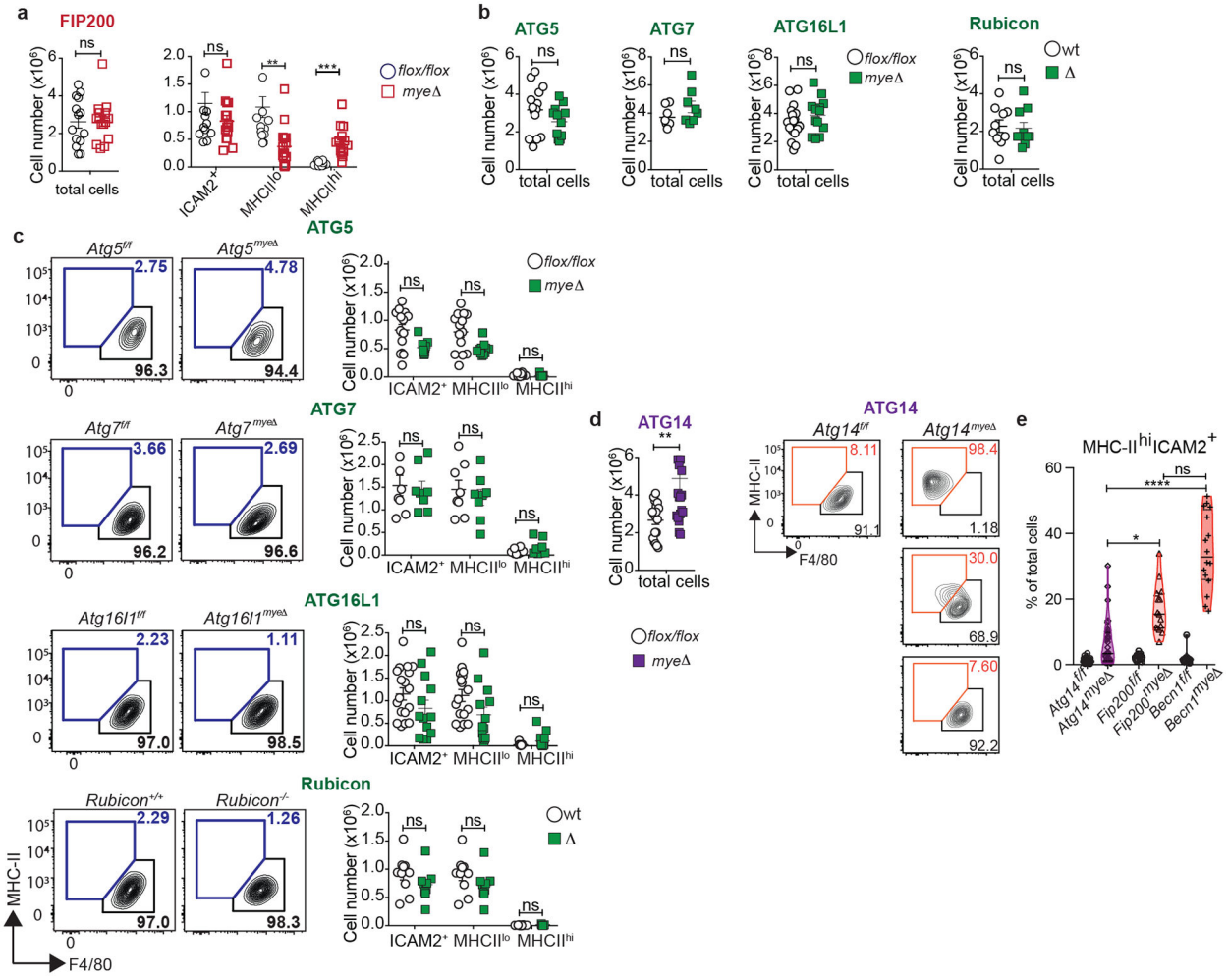

Extended Data Fig. 3. Alterations of peritoneal tissue resident macrophages in mice with central autophagy gene deficiency.

a, **b**, **c**, **d**, Quantification of number of total cells, total ICAM2$^+$ macrophages, and numbers of MHC-II^{high} and MHC-II^{low} fractions of ICAM2$^+$ macrophages from peritoneum lavage of mice harboring myeloid deficiency (*myeΔ)* in multiple autophagy genes and total deficiency (Δ) of Rubicon. (Data pooled from ≥3 independent experiments: *Fip200*$^{f/f}$, *n*=14; *Fip200*^{myeΔ}, *n*=16; *Atg5*$^{f/f}$, *n*=14; *Atg5*^{myeΔ}, *n*=12; *Atg7*$^{f/f}$, *n*=8; *Atg7*^{myeΔ}, *n*=8; *Atg16l1*$^{f/f}$, *n*=18; *Atg16l1*^{myeΔ}, *n*=13; *Rubicon* WT, *n=10; Rubicon* KO, *n=9; Atg14*$^{f/f}$, *n*=16; *Atg14*^{myeΔ}, *n*=15 mice; mean ± SEM; *P*, or P_{adj} for multiple comparison, with 2-tailed t test).

e, Violin plot showing percent of MHC-II^{high}ICAM2$^+$ macrophages in total peritoneal immune cells (*Atg14*$^{f/f}$, *n*=42; *Atg14*^{myeΔ}, *n*=38; *Becn1*$^{f/f}$, *n*=12; *Becn1*^{myeΔ}, *n*=16; *Fip200*$^{f/f}$, *n*=15; *Fip200*^{myeΔ}, *n*=15; mean ± SEM; P_{adj} by Kruskal-Wallis Dunn's multiple comparison test).

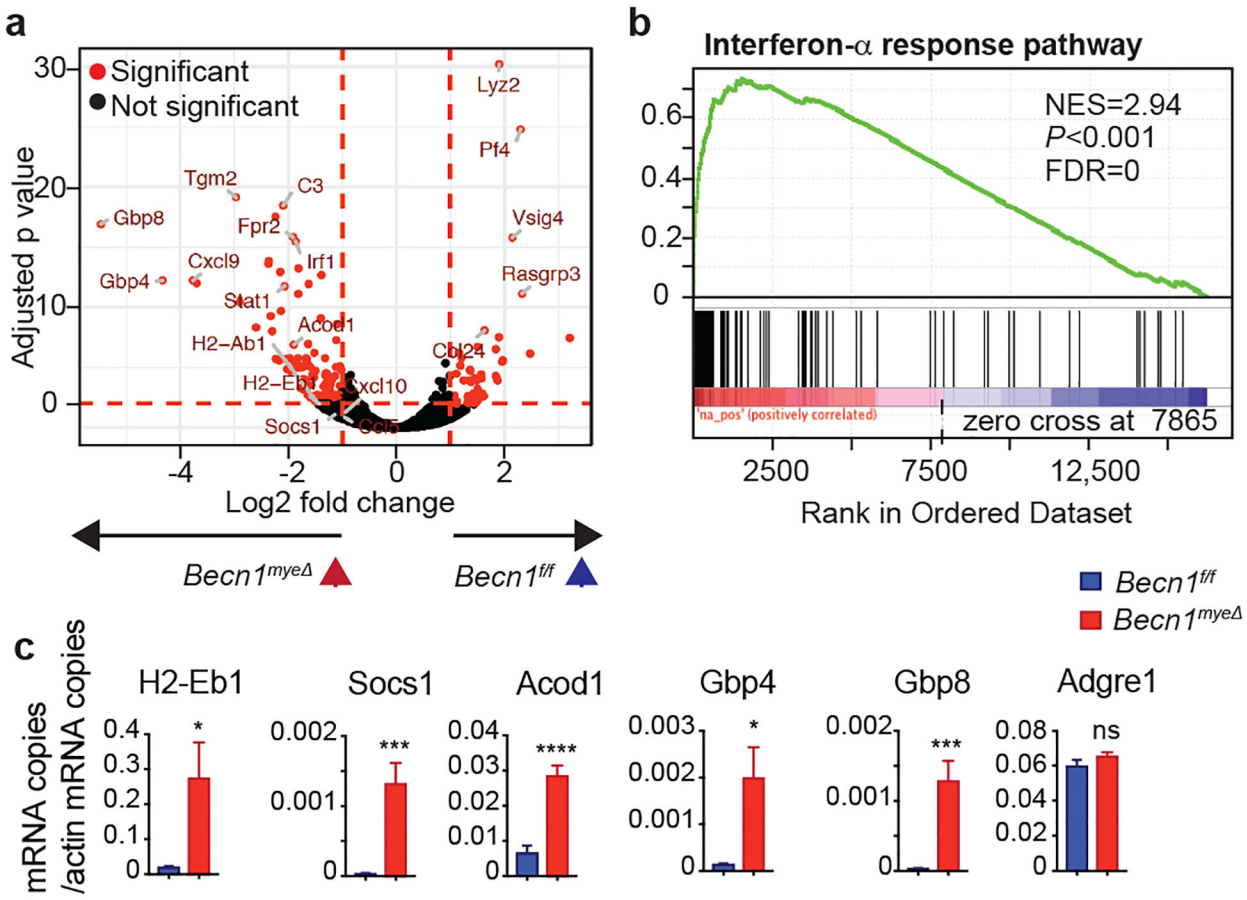

Extended Data Fig. 4. Beclin 1 deficiency augmented baseline macrophage IFN signaling.

a, Volcano plot shows genes upregulated in macrophages from *Becn1*^{myeΔ} mice on the left and downregulated on the right in RNA-seq data set (*Becn1*$^{f/f}$, *n*=4; *Becn1*^{myeΔ}, *n*=4).

b, Gene set enrichment analysis of *Becn1* dependent signature. (The green curve represents the density of the genes identified in the RNAseq with Normalized Enrichment Score (NES), *P* value and False Discovery Rate (FDR) listed.)

c, Transcript levels of the indicated genes in naïve peritoneal macrophages. (3 independent experiments, *Becn1*$^{f/f}$, *n*=9; *Becn1*^{myeΔ}, *n*=8; mean ± SEM; *P* by 2-tailed t test.)

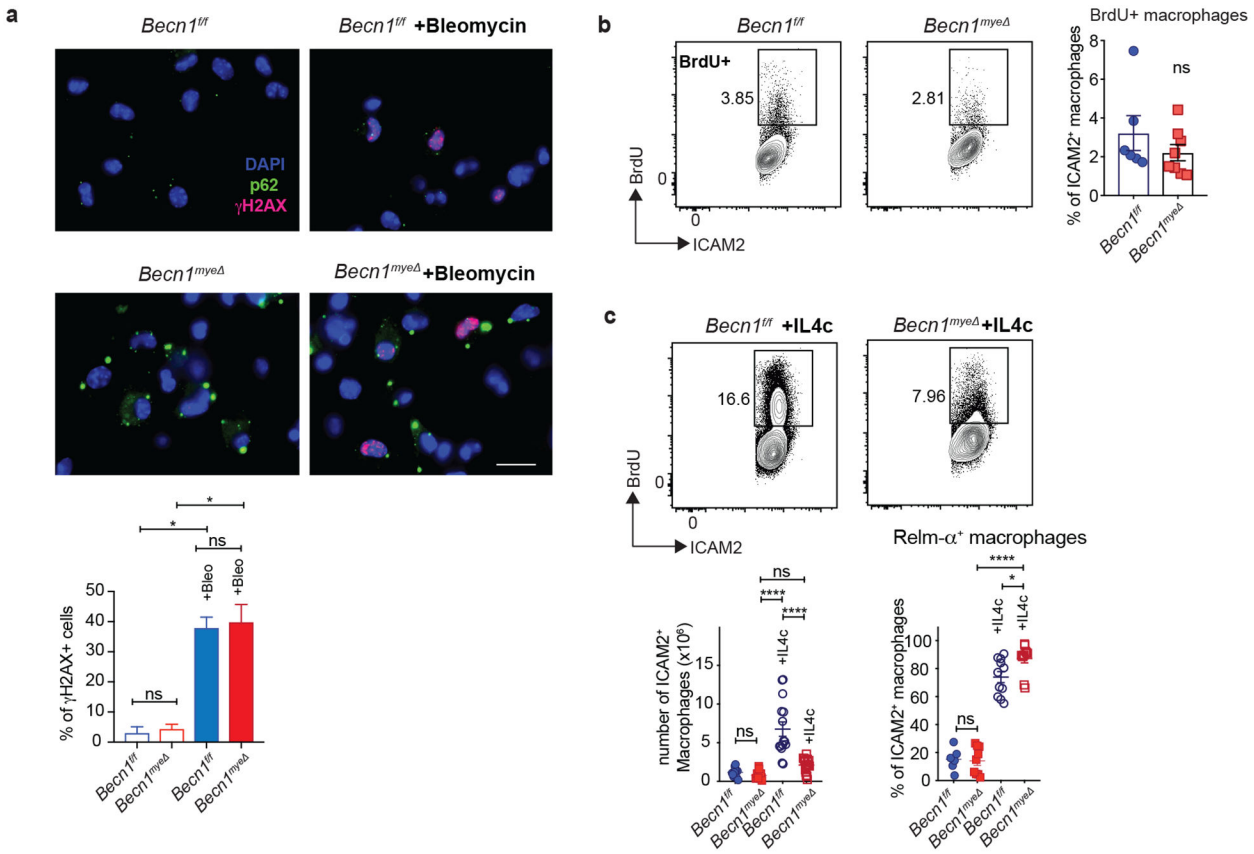

Extended Data Fig. 5. DNA damage response and cell proliferation of Beclin 1 deficient peritoneal macrophages.

a, The presence of DNA double-strand break were revealed by immunofluorescence for γ-H2AX (red) in peritoneal macrophages treated with Bleomycin for 6 hours or untreated p62 is stained in green and nuclei were labeled by DAPI (blue). Cells displaying ≥10 γ-H2AX foci were counted as positive. (Data represents 2 independent experiments; n=4, mean ±SEM; P by 2-tailed t test.)

b, Flow cytometry of BrdU incorporation by WT and Beclin 1-deficient ICAM2$^+$ macrophages. (2 independent experiments; *Becn1*$^{f/f}$, n=6 vs. *Becn1*^{myeΔ}, n=8; mean ±SEM; not significant by 2-tailed t test.)

c, WT and Beclin 1-deficient ICAM2$^+$ macrophages were enumerated after IL-4c injections (3 independent experiments; *Becn1*$^{f/f}$+PBS, n=11; *Becn1*^{myeΔ}+PBS, n=16; *Becn1*$^{f/f}$+IL4c, n=11; *Becn1*^{myeΔ}+ IL4c, n=19), and analyzed for frequency of BrdU$^+$ and RELMα level (2 independent experiments; *Becn1*$^{f/f}$+PBS, n=6; *Becn1*^{myeΔ}+PBS, n=9; *Becn1*$^{f/f}$+IL4c, n=11; *Becn1*^{myeΔ}+ IL4c, n=11; mean ± SEM; P_{adj} by Tukey's multiple comparisons test.)

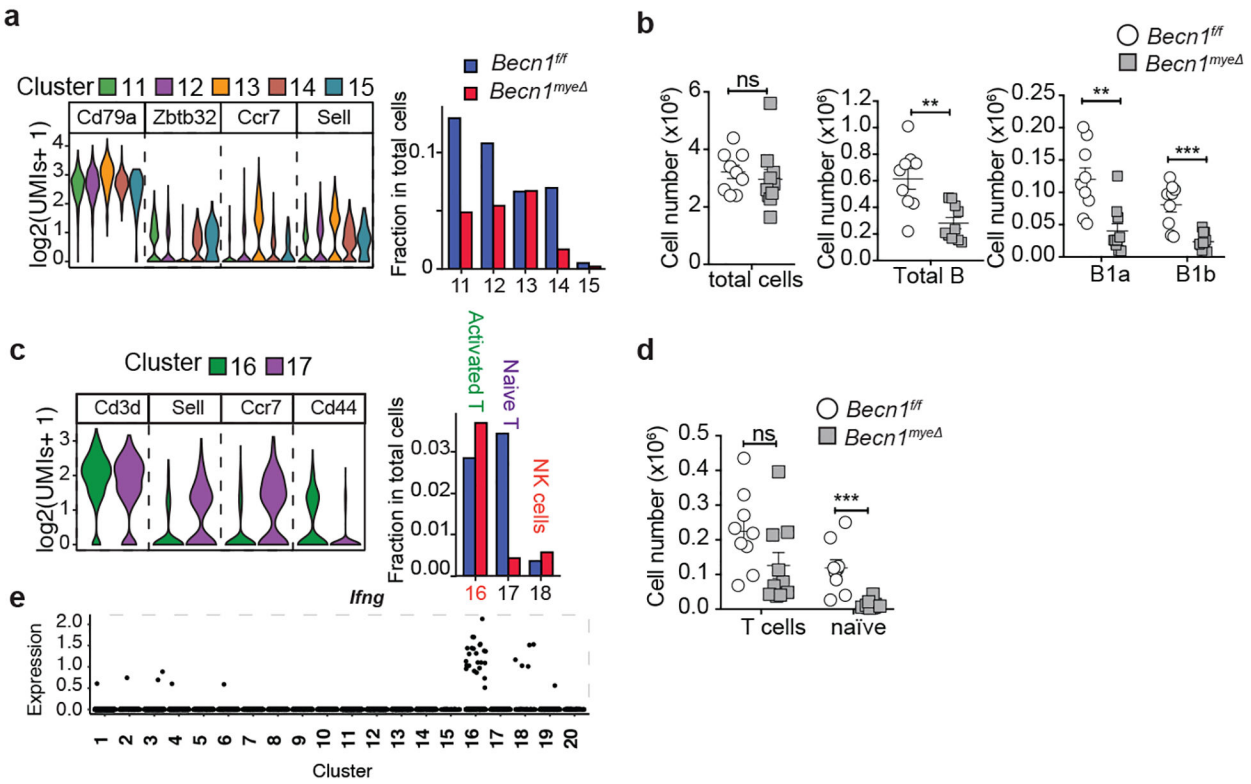

Extended Data Fig. 6. Peritoneal lymphocytes changes revealed by Single-cell RNA sequencing.

a and **c**, Violin plots showing the expression of marker genes of B (**a**) and T (**c**) cells clusters by single cell RNAseq. Bar graph comparing fraction size of clusters.

b and **d** Flow cytometry validation on naïve mice (*Becn1*$^{f/f}$, n=9; *Becn1*^{myeΔ}, n=10; mean ± SEM; P, and P_{adj} for multiple comparison, by 2-tailed t test).

e, *Ifng* transcript level among clusters revealed by single cell RNAseq.

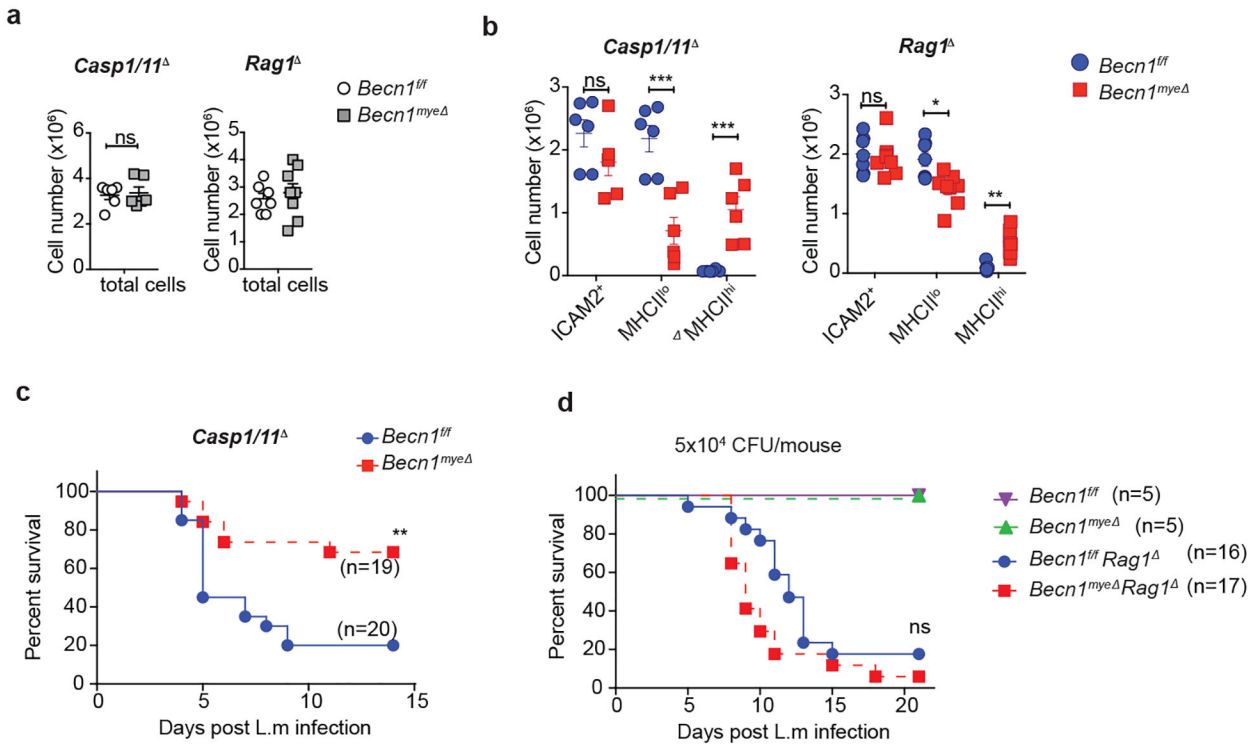

Extended Data Fig. 7. Peritoneal macrophage activation in *Becn1*^{myeΔ} mice is independent of inflammasome and adaptive immune response.

a and **b**, Peritoneal macrophages obtained from naïve mice were analyzed for total cells (**a**), total ICAM2^{+} macrophages, MHC-II^{high} and MHC-II^{low} fractions of ICAM2^{+} macrophages (**b**) by flow cytometry (*Becn1*$^{f/f}$*Casp1/11*^{Δ}, n=6; *Becn1*^{myeΔ}*Casp1/11*^{Δ}, n=6; *Becn1*$^{f/f}$*Rag1*^{Δ}, n=7; *Becn1*^{myeΔ}*Rag1*^{Δ}, n=8 mice, mean ± SEM, P and P_{adj} by unpaired 2-tailed t test).

c and **d**, Survival of mice after i.p. inoculation of 5×10^{5} CFUs (**c**) or 5×10^{4} CFU (**d**) of *L. monocytogenes* (Data pooled from 3–4 experiments, P by Log-rank Mantel-Cox test).

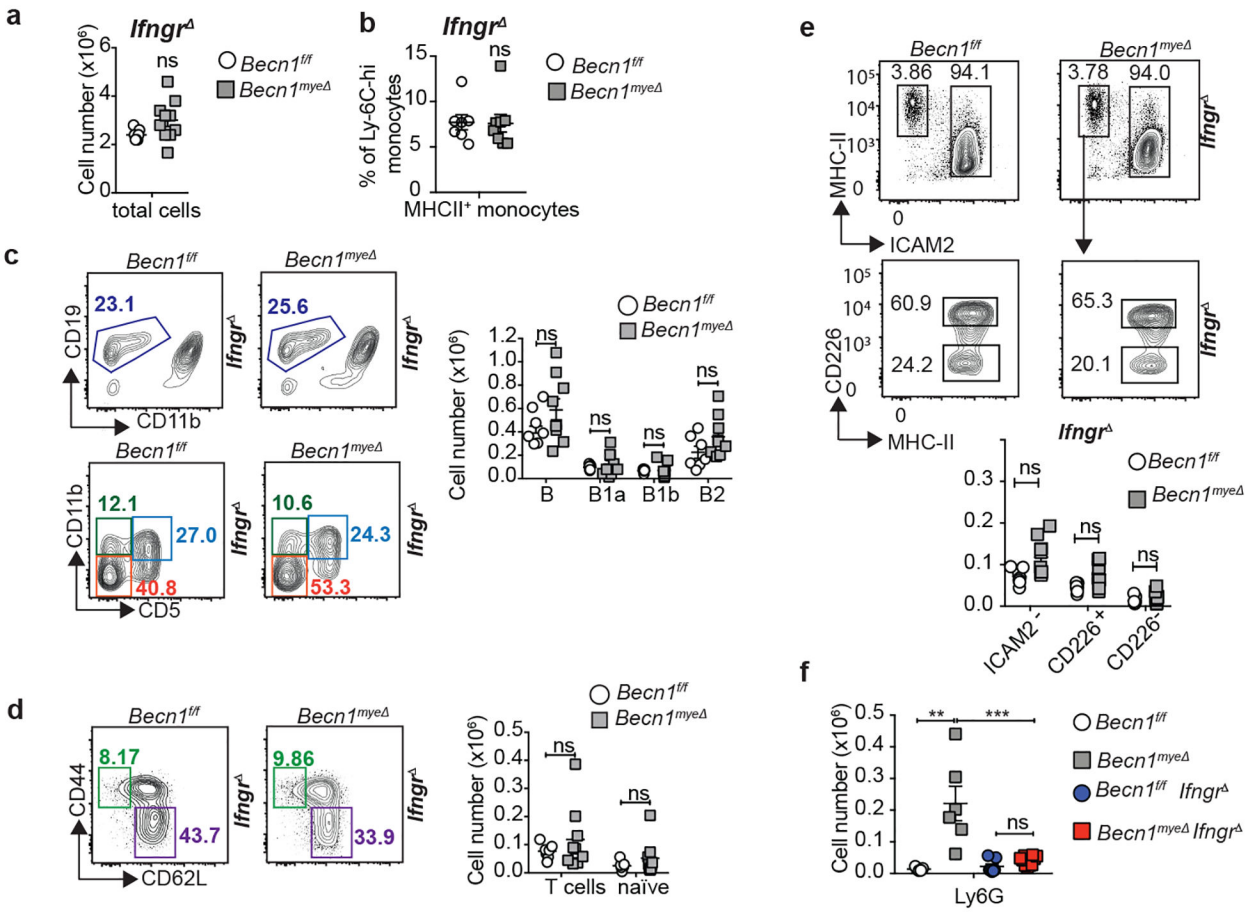

Extended Data Fig. 8. *Ifngr*$^{\Delta}$ rescues peritoneal immune cell homeostasis in *Becn1*^{myeΔ} mice.

a-**e**, Flow cytometry analysis of total cells (**a**), B cells (**b**), T cells (**c**), SPM and monocytes (**d**), and peritoneal neutrophils (**e**) and obtained from naïve mice of the indicated genotypes. (Data are from 2 independent experiments; *Becn1*$^{f/f}$, n=8 vs. *Becn1*^{myeΔ}, n=9; mean ± SEM; not significant by 2-tailed Mann-Whitney test.)

f, Blood neutrophils were analyzed by flow cytometry. (n=6; mean ± SEM; P by 2-tailed Mann-Whitney test.)

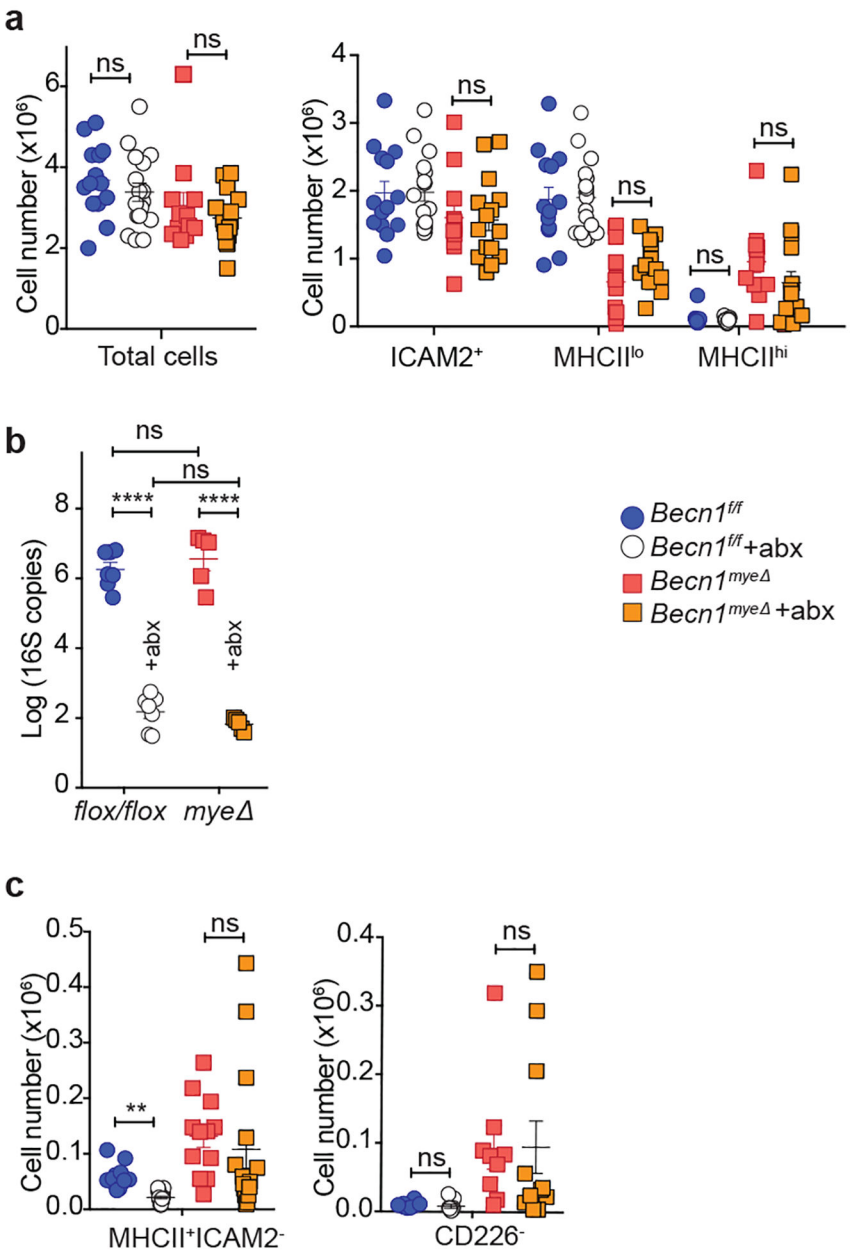

Extended Data Fig. 9. Peritoneal macrophage activation in *Becn1*^{myeΔ} mice is independent of the presence of microbiota.

a and **c**, Quantification of total peritoneal cells and ICAM2^{+} macrophages (**a**) and numbers of ICAM2^{-} macrophages and CD226^{-} fraction of ICAM2^{-} macrophages (**c**) (P_{adj} by Dunn's multiple comparisons test). *Becn1*$^{f/f}$(Kool-Aid), n=7; *Becn1*$^{f/f}$(abx), n=9; *Becn1*^{myeΔ}(Kool-Aid), n=9; *Becn1*^{myeΔ}(abx), n=10; mean ± SEM, P_{adj} by 1way ANOVA with Dunn's multiple comparisons test). **b**, Quantification of 16S copy number from stool samples of mice. (*Becn1*$^{f/f}$, n=7 each for kool-aid and abx vs. *Becn1*^{myeΔ}, n=5 each for kool-aid and abx; mean ± SEM, P_{adj} analyzed by Tukey's multiple comparisons test).

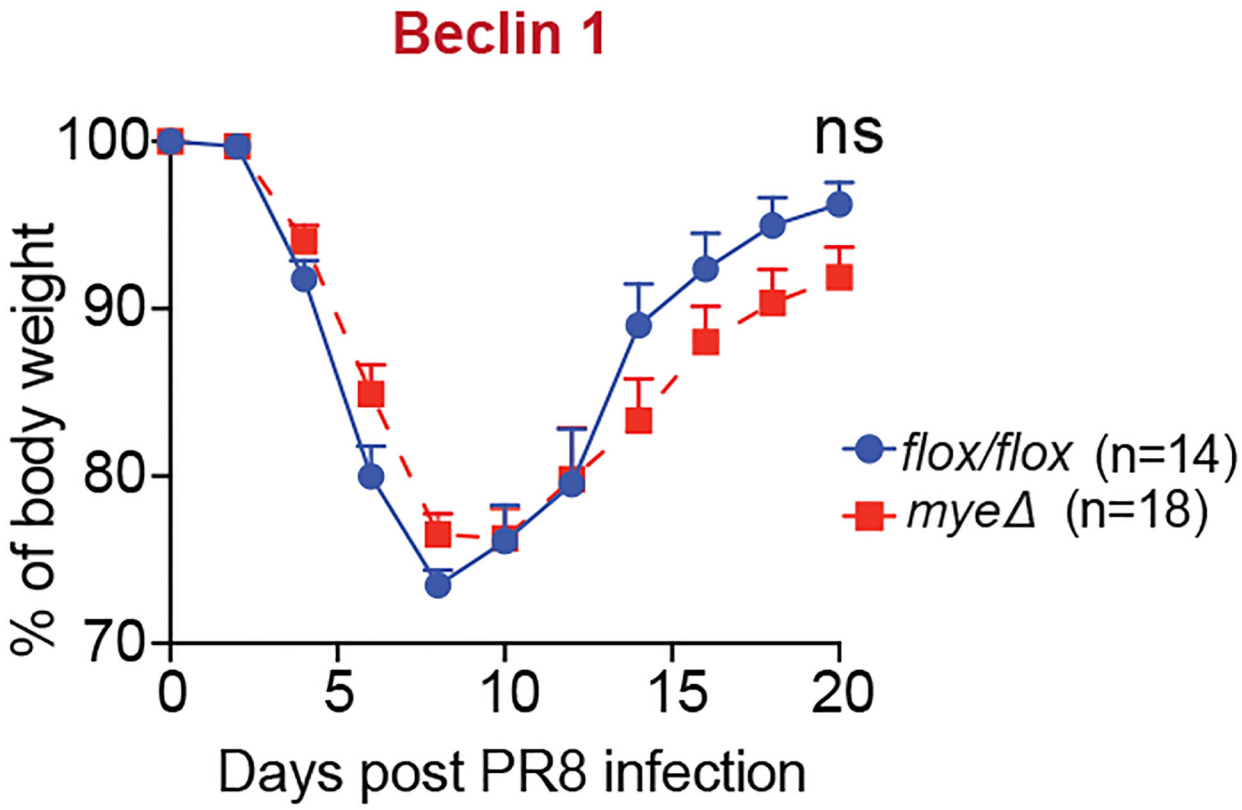

Extended Data Fig. 10. *Becn1*^{myeΔ} mice did not exhibit enhanced resistance to pulmonary influenza infection.

Mice were infected intranasally with 250 TCID50 Influenza A PR8 and monitored for weight loss. (Data pooled from 4 independent experiments, mean ± SEM, not significant by 2way ANOVO for the whole curve or by 2-tailed t test for each time point).

Supplementary Material

Refer to Web version on PubMed Central for supplementary material.

Acknowledgements

We thank Gwendolyn Randolph, Brian Edelson, Deepta Bhattacharya and the former members of the Virgin lab for discussion. The authors thank Jonathan Brestoff and Sytse Piersma for manuscript review and thank Christine Yokoyama and Hongju Deng for technical assistance. Technical support was from McDonnell Genome Institute, Genome Technology Access Center, Flow Cytometry Core Facility, Molecular Microbiology Imaging Facility, Pulmonary Morphology Core, and Center for Human Immunology & Immunotherapy Programs at Washington University School of Medicine. The research was supported by NIH grant U19 AI109725 and the Crohn's and Colitis Foundation grant #326556 (to H.W.V.), NIH grant U19 AI42784 (to H.W.V. and C.L.S.), and NIH grant R01 AI132697 (to C.L.S.). Authors receive supports from MES of Russia (project 2.3300.2017/4.6 to K.Z.); NIH K08 (A128043 to C.B.W.); Pediatric Infectious Diseases Society/St. Jude Children's Research Hospital fellowship in basic research (to A.O.); Young Investigators Grant for Probiotics Research from the Global Probiotics Council (to M.T.B.); Burroughs Wellcome Fund Investigators in the Pathogenesis of Infectious Disease (to C.L.S.).

Reference:

1. Barton ES et al. Herpesvirus latency confers symbiotic protection from bacterial infection. Nature 447, 326–329, doi:10.1038/nature05762 (2007). [PubMed: 17507983]

2. Netea MG et al. Trained immunity: A program of innate immune memory in health and disease. Science 352, aaf1098, doi:10.1126/science.aaf1098 (2016).
3. Medzhitov R Origin and physiological roles of inflammation. Nature 454, 428–435, doi:10.1038/nature07201 (2008). [PubMed: 18650913]
4. Mizushima N & Komatsu M Autophagy: renovation of cells and tissues. Cell 147, 728–741, doi:10.1016/j.cell.2011.10.026 (2011). [PubMed: 22078875]
5. Cadwell K et al. A key role for autophagy and the autophagy gene Atg16l1 in mouse and human intestinal Paneth cells. Nature 456, 259–263, doi:10.1038/nature07416 (2008). [PubMed: 18849966]
6. Saitoh T et al. Loss of the autophagy protein Atg16L1 enhances endotoxin-induced IL-1beta production. Nature 456, 264–268 (2008). [PubMed: 18849965]
7. Levine B, Mizushima N & Virgin HW Autophagy in immunity and inflammation. Nature 469, 323–335, doi:10.1038/nature09782 (2011). [PubMed: 21248839]
8. Kimmey JM et al. Unique role for ATG5 in neutrophil-mediated immunopathology during M. tuberculosis infection. Nature 528, 565–569, doi:10.1038/nature16451 (2015). [PubMed: 26649827]
9. Lu Q et al. Homeostatic Control of Innate Lung Inflammation by Vici Syndrome Gene Epg5 and Additional Autophagy Genes Promotes Influenza Pathogenesis. Cell Host Microbe 19, 102–113, doi:10.1016/j.chom.2015.12.011 (2016). [PubMed: 26764600]
10. Park S et al. Autophagy Genes Enhance Murine Gammaherpesvirus 68 Reactivation from Latency by Preventing Virus-Induced Systemic Inflammation. Cell host & microbe 19, 91–101, doi:10.1016/j.chom.2015.12.010 (2016). [PubMed: 26764599]
11. Martinez J et al. Noncanonical autophagy inhibits the autoinflammatory, lupus-like response to dying cells. Nature 533, 115–119, doi:10.1038/nature17950 (2016). [PubMed: 27096368]
12. Cunha LD et al. LC3-Associated Phagocytosis in Myeloid Cells Promotes Tumor Immune Tolerance. Cell 175, 429–441 e416, doi:10.1016/j.cell.2018.08.061 (2018). [PubMed: 30245008]
13. Huang S et al. Immune response in mice that lack the interferon-gamma receptor. Science 259, 1742–1745 (1993). [PubMed: 8456301]
14. Unanue ER Inter-relationship among macrophages, natural killer cells and neutrophils in early stages of Listeria resistance. Curr.Opin.Immunol 9, 35–43 (1997). [PubMed: 9039774]
15. Yoshikawa Y et al. Listeria monocytogenes ActA-mediated escape from autophagic recognition. Nat Cell Biol 11, 1233–1240, doi:10.1038/ncb1967 (2009). [PubMed: 19749745]
16. Yano T et al. Autophagic control of listeria through intracellular innate immune recognition in drosophila. Nat.Immunol 9, 908–916 (2008). [PubMed: 18604211]
17. Zhao Z et al. Autophagosome-independent essential function for the autophagy protein Atg5 in cellular immunity to intracellular pathogens. Cell host & microbe 4, 458–469 (2008). [PubMed: 18996346]
18. Meyer-Morse N et al. Listeriolysin O is necessary and sufficient to induce autophagy during Listeria monocytogenes infection. PLoS One 5, e8610, doi:10.1371/journal.pone.0008610 (2010). [PubMed: 20062534]
19. Huang J & Brumell JH Bacteria-autophagy interplay: a battle for survival. Nat Rev Microbiol 12, 101–114, doi:10.1038/nrmicro3160 (2014). [PubMed: 24384599]
20. Liang XH et al. Induction of autophagy and inhibition of tumorigenesis by beclin 1. Nature 402, 672–676 (1999). [PubMed: 10604474]
21. Choi J et al. The parasitophorous vacuole membrane of Toxoplasma gondii is targeted for disruption by ubiquitin-like conjugation systems of autophagy. Immunity 40, 924–935, doi:10.1016/j.immuni.2014.05.006 (2014). [PubMed: 24931121]
22. Mitchell G et al. Listeria monocytogenes triggers noncanonical autophagy upon phagocytosis, but avoids subsequent growth-restricting xenophagy. Proc Natl Acad Sci U S A 115, E210–E217, doi:10.1073/pnas.1716055115 (2018). [PubMed: 29279409]
23. Cain DW et al. Identification of a tissue-specific, C/EBPbeta-dependent pathway of differentiation for murine peritoneal macrophages. J Immunol 191, 4665–4675, doi:10.4049/jimmunol.1300581 (2013). [PubMed: 24078688]

24. Galluzzi L et al. Autophagy in malignant transformation and cancer progression. EMBO J 34, 856–880, doi:10.15252/embj.201490784 (2015). [PubMed: 25712477]
25. Martinez J et al. Molecular characterization of LC3-associated phagocytosis reveals distinct roles for Rubicon, NOX2 and autophagy proteins. Nature cell biology 17, 893–906, doi:10.1038/ncb3192 (2015). [PubMed: 26098576]
26. Hartlova A et al. DNA damage primes the type I interferon system via the cytosolic DNA sensor STING to promote anti-microbial innate immunity. Immunity 42, 332–343, doi:10.1016/j.immuni.2015.01.012 (2015). [PubMed: 25692705]
27. Liang Q et al. Crosstalk between the cGAS DNA sensor and Beclin-1 autophagy protein shapes innate antimicrobial immune responses. Cell Host Microbe 15, 228–238, doi:10.1016/j.chom.2014.01.009 (2014). [PubMed: 24528868]
28. Rodier F et al. Persistent DNA damage signalling triggers senescence-associated inflammatory cytokine secretion. Nat Cell Biol 11, 973–979, doi:10.1038/ncb1909 (2009). [PubMed: 19597488]
29. West AP et al. Mitochondrial DNA stress primes the antiviral innate immune response. Nature 520, 553–557, doi:10.1038/nature14156 (2015). [PubMed: 25642965]
30. Jenkins SJ et al. Local macrophage proliferation, rather than recruitment from the blood, is a signature of TH2 inflammation. Science 332, 1284–1288, doi:10.1126/science.1204351 (2011). [PubMed: 21566158]
31. Gautier EL et al. Gata6 regulates aspartoacylase expression in resident peritoneal macrophages and controls their survival. J Exp Med 211, 1525–1531, doi:10.1084/jem.20140570 (2014). [PubMed: 25024137]
32. Rosas M et al. The transcription factor Gata6 links tissue macrophage phenotype and proliferative renewal. Science 344, 645–648, doi:10.1126/science.1251414 (2014). [PubMed: 24762537]
33. Okabe Y & Medzhitov R Tissue-specific signals control reversible program of localization and functional polarization of macrophages. Cell 157, 832–844, doi:10.1016/j.cell.2014.04.016 (2014). [PubMed: 24792964]
34. Bain CC et al. Long-lived self-renewing bone marrow-derived macrophages displace embryo-derived cells to inhabit adult serous cavities. Nat Commun 7, ncomms11852, doi:10.1038/ncomms11852 (2016).
35. Mabbott NA & Gray D Identification of co-expressed gene signatures in mouse B1, marginal zone and B2 B-cell populations. Immunology 141, 79–95, doi:10.1111/imm.12171 (2014). [PubMed: 24032749]
36. Ansel KM, Harris RB & Cyster JG CXCL13 is required for B1 cell homing, natural antibody production, and body cavity immunity. Immunity 16, 67–76 (2002). [PubMed: 11825566]
37. Shi CS et al. Activation of autophagy by inflammatory signals limits IL-1beta production by targeting ubiquitinated inflammasomes for destruction. Nature immunology 13, 255–263, doi:10.1038/ni.2215 (2012). [PubMed: 22286270]
38. Nakahira K et al. Autophagy proteins regulate innate immune responses by inhibiting the release of mitochondrial DNA mediated by the NALP3 inflammasome. Nature immunology 12, 222–230, doi:10.1038/ni.1980 (2011). [PubMed: 21151103]
39. Santeford A et al. Impaired autophagy in macrophages promotes inflammatory eye disease. Autophagy, 1–10, doi:10.1080/15548627.2016.1207857 (2016). [PubMed: 26799652]
40. Auerbuch V, Brockstedt DG, Meyer-Morse N, O'Riordan M & Portnoy D Mice lacking the type I interferon receptor are resistant to Listeria monocytogenes. J Exp Med 200, 527–533, doi:10.1084/jem.20040976 (2004). [PubMed: 15302899]
41. Carrero JA, Calderon B & Unanue ER Type I interferon sensitizes lymphocytes to apoptosis and reduces resistance to Listeria infection. J Exp Med 200, 535–540, doi:10.1084/jem.20040769 (2004). [PubMed: 15302900]
42. O'Connell RM et al. Type I interferon production enhances susceptibility to Listeria monocytogenes infection. J Exp Med 200, 437–445, doi:10.1084/jem.20040712 (2004). [PubMed: 15302901]
43. Pitts MG, Myers-Morales T & D'Orazio SE Type I IFN Does Not Promote Susceptibility to Foodborne Listeria monocytogenes. J Immunol 196, 3109–3116, doi:10.4049/jimmunol.1502192 (2016). [PubMed: 26895837]

44. Martin PK et al. Autophagy proteins suppress protective type I interferon signalling in response to the murine gut microbiota. Nat Microbiol 3, 1131–1141, doi:10.1038/s41564-018-0229-0 (2018). [PubMed: 30202015]
45. Abt MC et al. Commensal bacteria calibrate the activation threshold of innate antiviral immunity. Immunity 37, 158–170, doi:10.1016/j.immuni.2012.04.011 (2012). [PubMed: 22705104]
46. Ichinohe T et al. Microbiota regulates immune defense against respiratory tract influenza A virus infection. Proc Natl Acad Sci U S A 108, 5354–5359, doi:10.1073/pnas.1019378108 (2011). [PubMed: 21402903]
47. Steed AL et al. The microbial metabolite desaminotyrosine protects from influenza through type I interferon. Science 357, 498–502, doi:10.1126/science.aam5336 (2017). [PubMed: 28774928]
48. Kim KW et al. MHC II+ resident peritoneal and pleural macrophages rely on IRF4 for development from circulating monocytes. J Exp Med 213, 1951–1959, doi:10.1084/jem.20160486 (2016). [PubMed: 27551152]
49. Kanayama M, He YW & Shinohara ML The lung is protected from spontaneous inflammation by autophagy in myeloid cells. Journal of immunology 194, 5465–5471, doi:10.4049/jimmunol.1403249 (2015).
50. Biering SB et al. Viral Replication Complexes Are Targeted by LC3-Guided Interferon-Inducible GTPases. Cell Host Microbe 22, 74–85 e77, doi:10.1016/j.chom.2017.06.005 (2017). [PubMed: 28669671]
51. DeSelm CJ et al. Autophagy proteins regulate the secretory component of osteoclastic bone resorption. Developmental cell 21, 966–974, doi:10.1016/j.devcel.2011.08.016 (2011). [PubMed: 22055344]
52. Medina DL et al. Transcriptional activation of lysosomal exocytosis promotes cellular clearance. Dev Cell 21, 421–430, doi:10.1016/j.devcel.2011.07.016 (2011). [PubMed: 21889421]
53. Tsuboyama K et al. The ATG conjugation systems are important for degradation of the inner autophagosomal membrane. Science (New York, N.Y.), doi:10.1126/science.aaf6136 (2016).
54. Kuma A, Komatsu M & Mizushima N Autophagy-monitoring and autophagy-deficient mice. Autophagy 13, 1619–1628, doi:10.1080/15548627.2017.1343770 (2017). [PubMed: 28820286]
55. Fernandez AF et al. Disruption of the beclin 1-BCL2 autophagy regulatory complex promotes longevity in mice. Nature 558, 136–140, doi:10.1038/s41586-018-0162-7 (2018). [PubMed: 29849149]
56. Miller BC et al. The autophagy gene ATG5 plays an essential role in B lymphocyte development. Autophagy 4, 309–314 (2008). [PubMed: 18188005]
57. Sanjuan MA et al. Toll-like receptor signaling in macrophages links the autophagy pathway to phagocytosis. Nature 450, 1253–1257 (2007). [PubMed: 18097414]
58. Gan B et al. Role of FIP200 in cardiac and liver development and its regulation of TNFalpha and TSC-mTOR signaling pathways. The Journal of cell biology 175, 121–133 (2006). [PubMed: 17015619]
59. Hwang S et al. Nondegradative role of Atg5-Atg12/Atg16L1 autophagy protein complex in antiviral activity of interferon gamma. Cell Host Microbe 11, 397–409, doi:10.1016/j.chom.2012.03.002 (2012). [PubMed: 22520467]
60. MacDuff DA et al. Phenotypic complementation of genetic immunodeficiency by chronic herpesvirus infection. Elife 4, doi:10.7554/eLife.04494 (2015).
61. Jarjour NN et al. Bhlhe40 mediates tissue-specific control of macrophage proliferation in homeostasis and type 2 immunity. Nat Immunol 20, 687–700, doi:10.1038/s41590-019-0382-5 (2019). [PubMed: 31061528]
62. Love MI, Huber W & Anders S Moderated estimation of fold change and dispersion for RNA-seq data with DESeq2. Genome Biol 15, 550, doi:10.1186/s13059-014-0550-8 (2014). [PubMed: 25516281]
63. Baldridge MT et al. Commensal microbes and interferon-lambda determine persistence of enteric murine norovirus infection. Science 347, 266–269, doi:10.1126/science.1258025 (2015). [PubMed: 25431490]
64. Gluschko A et al. The β2 integrin mac-1 induces protective LC3-associated phagocytosis of Listeria monocytogenes. Cell Host Microbe 23, 324–337 (2018). [PubMed: 29544096]

65. Lee HK et al. In vivo requirement for Atg5 in antigen presentation by dendritic cells. Immunity 32, 227–239 (2010). [PubMed: 20171125]

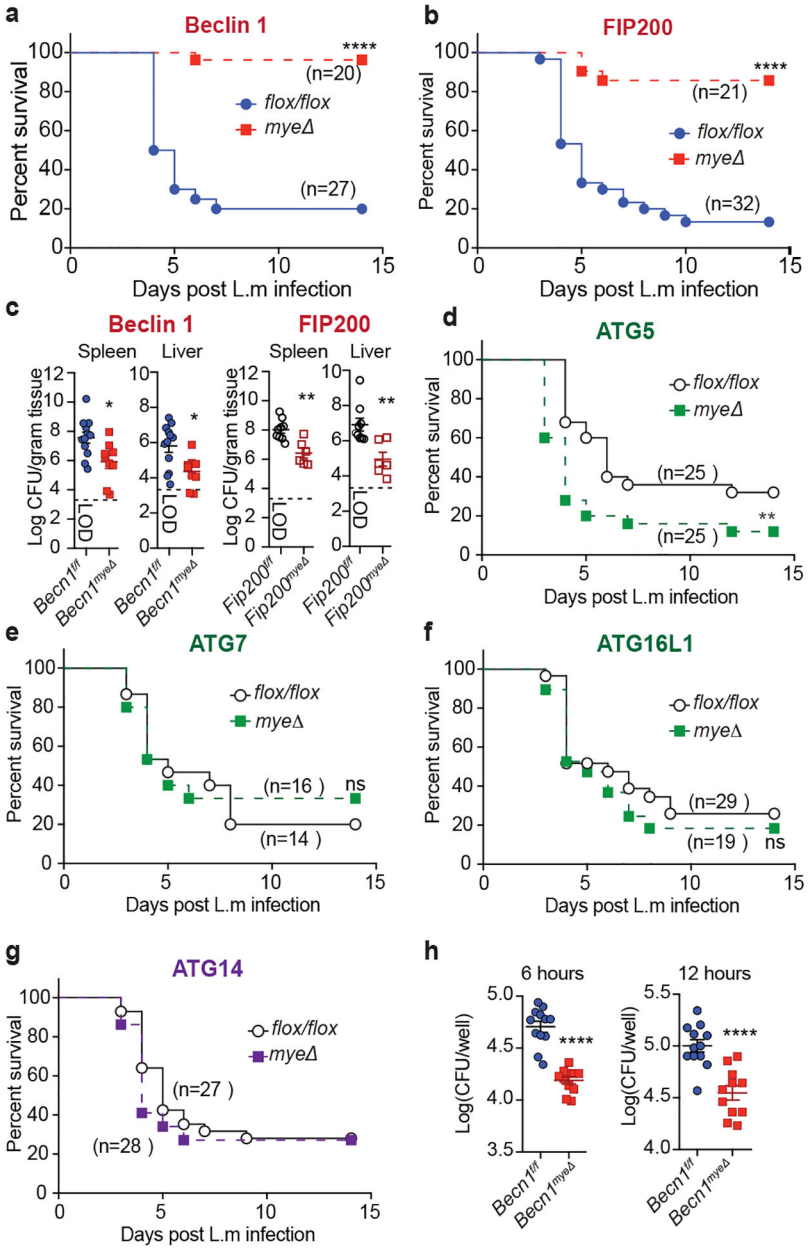

Figure 1. Mice with deficiencies of certain autophagy genes in myeloid cells display enhanced resistance to *L. monocytogenes*.

a, **b** and **d**, **e**, **f**, **g**, Survival of mice harboring myeloid deficiency (*myeΔ*) in autophagy genes vs littermate controls, after i.p. inoculation with 4~5×10^5 colony forming units (CFUs) of *L. monocytogenes* (Data pooled from 3–4 experiments, *P* by Log-rank Mantel-Cox test; Notable comparisons that were not significantly different are designated as *ns*). **c**, *L. monocytogenes* CFU in spleen and liver 3 days after infection (data pooled from 2 experiments, $Becn1^{f/f}$, *n*=12; $Becn1^{myeΔ}$ *n*=9; $Fip200^{f/f}$, *n*=9; $Fip200^{myeΔ}$ *n*=6 mice, mean ± SEM; *P* by two-tailed t test).

h, *Ex vivo* bactericidal activity of purified peritoneal macrophages at the indicated times (data pooled from 2 experiments, $Becn1^{f/f}$, n=12; $Becn1^{myeΔ}$ n=11, mean ± SEM; P_{adj} by two-tailed t test).

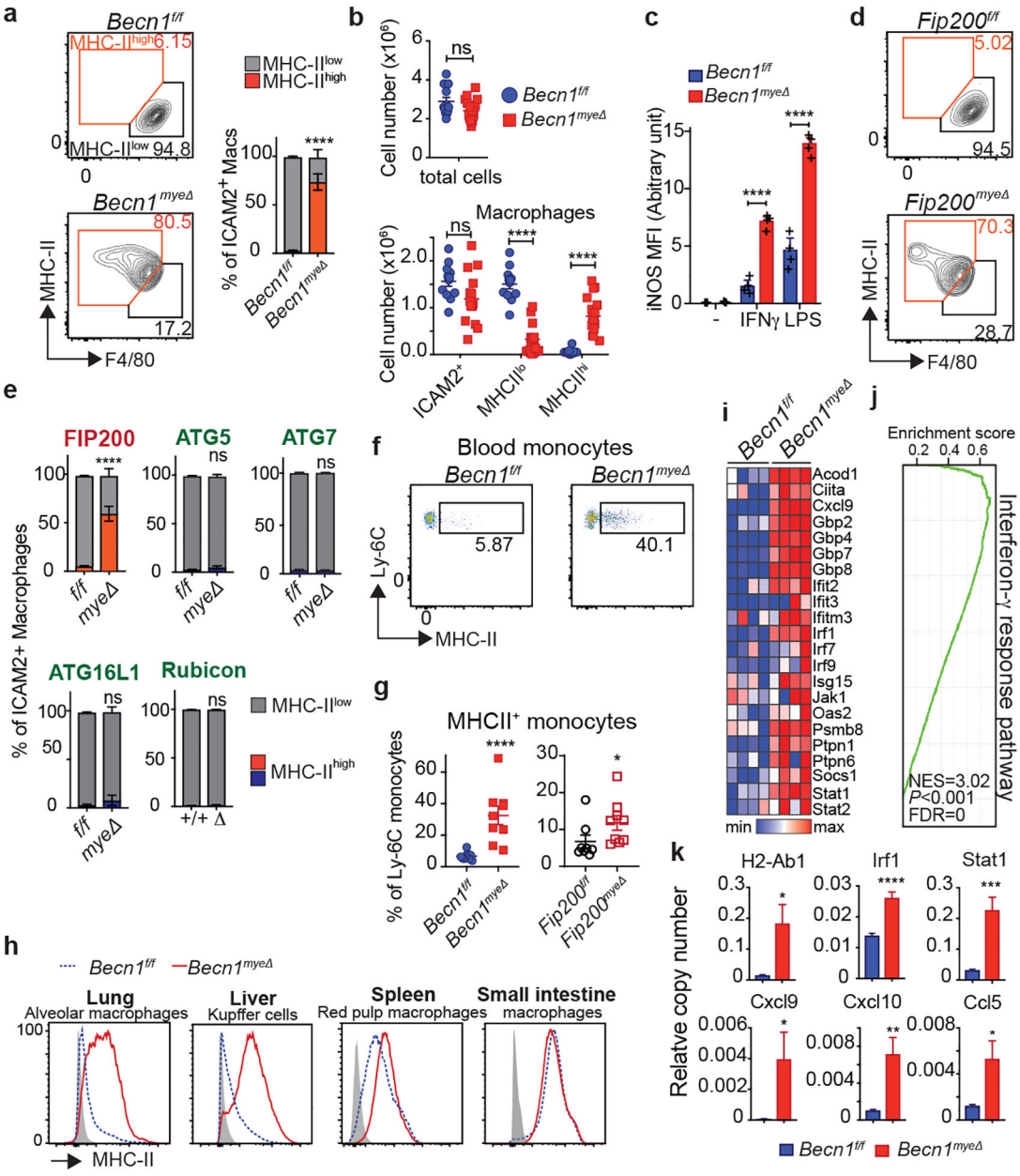

Figure 2. Alterations of peritoneal tissue-resident macrophages in mice with select autophagy gene deficiency.

a, **d**, Flow cytometry of macrophage subsets in peritoneum of adult mice ($n \geq 3$ independent experiments with $n \geq 3$ mice). Percentage of MHC-II^{low} and MHC-II^{high} macrophages in total ICAM2^{+} macrophages are shown in the bar graph (**a**) (*Becn1*$^{f/f}$, n=13; *Becn1*^{myeΔ}, n=15; mean ± SEM, P_{adj} by 2way ANOVA Sidak's multiple comparisons test on MHC-II^{high}).

b, Dot plots showing the number of the total cells, and total, MHC-II^{high}, and MHC-II^{low} fractions of ICAM2^{+} macrophages (data pooled from ≥3 experiments; *Becn1*$^{f/f}$, n=13; *Becn1*^{myeΔ}, n=15; mean ± SEM, P_{adj} by multiple t test).

c, *Ex vivo* stimulated peritoneal macrophages were analyzed for intracellular iNOS following stimulation (representative of 3 experiments, n=4; mean ± SEM, P_{adj} by multiple t test).

e, Percentage of MHC-II^{low} and MHC-II^{high} ICAM2^{+} macrophages (*Fip200*$^{f/f}$, n=14; *Fip200*^{myeΔ}, n=15; *Atg5*$^{f/f}$, n=10; *Atg5*^{myeΔ}, n=7; *Atg7*$^{f/f}$, n=4; *Atg7*^{myeΔ}, n=4; *Atg16l1*$^{f/f}$, n=6; *Atg16l1*^{myeΔ}, n=6; *Rubicon*$^{+/+}$, n=10; *Rubicon*$^{-/-}$, n=9 mice; mean ± SEM, P_{adj} by 2way ANOVA Sidak's multiple comparisons test on MHC-II^{high}).

f, flow cytometry analysis of MHC-II level on monocytes (2 experiments with n≥3 biological replicates each).

g, percentage of MHC-II^{+} monocytes (*Becn1*$^{f/f}$, n=9; *Becn1*^{myeΔ}, n=8; *Fip200*$^{f/f}$, n=8; *Fip200*^{myeΔ}, n=8 mice; mean ± SEM, P by two-tailed Mann-Whitney test).

h, flow cytometry analysis of tissue-resident macrophages (2 experiments with n≥3 biological replicates each).

i, Heatmap of selected genes regulated by Beclin 1 by RNAseq (n=4 samples each).

j, Gene set enrichment analysis of *Becn1* dependent signature (green curve represents the density of the genes identified in the RNAseq with Normalized Enrichment Score (NES), P value and False Discovery Rate (FDR) listed).

k, qRT-PCR measurements of transcript levels in naïve peritoneal macrophages (3 independent experiments, *Becn1*$^{f/f}$, n=9; *Becn1*^{myeΔ}, n=8; mean ± SEM, P by two-tailed Mann-Whitney test).

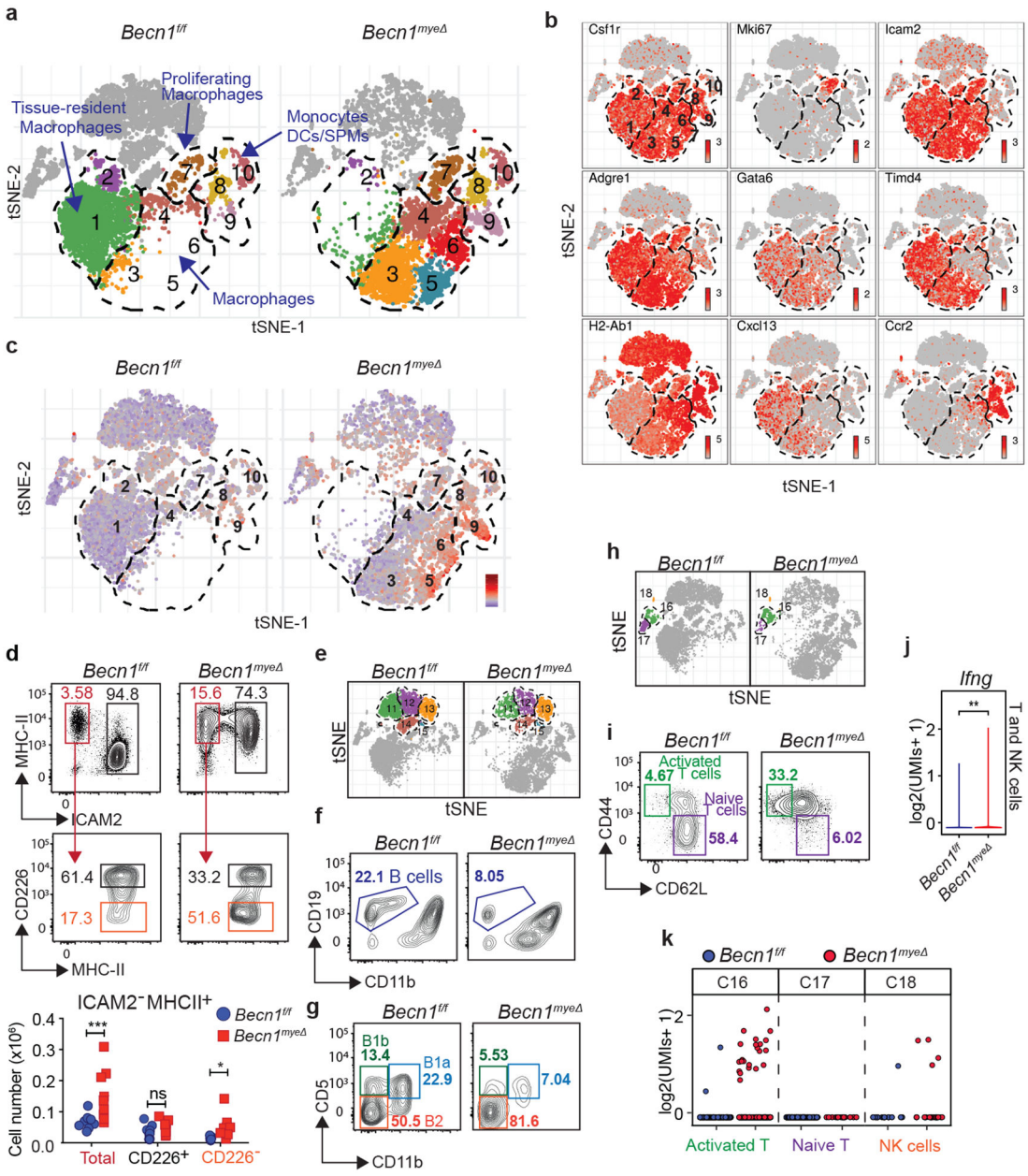

Figure 3. Disrupted immune cell homeostasis associated with *Becn1* myeloid deficiency.

a, b, c, e, h, Myeloid (SPM, small peritoneal macrophages) (**a**), B cells (**e**), T and NK cells (**h**) clusters from single-cell profiles of peritoneal cavity cells visualized with t-SNE ($n = 4$ naïve mice, 8 weeks old). Gene expression (**b**) and IFNγ pathway (**c**) was projected on the tSNE plots with 2 groups of mice overlaid in (**b**). Color scaled for each gene with highest log-normalized expression level noted.

d, Flow cytometry validation on naïve mice. (3 experiments, *Becn1*$^{f/f}$, n=8; *Becn1*^{myeΔ} n=9 mice; mean ± SEM, P_{adj} by 2way ANOVA Sidak's multiple comparisons test).

f, **g**, **i**, Flow cytometry analysis on naïve mice (3 experiments, $n \geq 3$ mice each).

j, **k**, Violin and dot plots of *Ifng* expressing T and NK cells clusters of sc-RNAseq data set (**P_{adj} <0.01, MAST differential expression test).

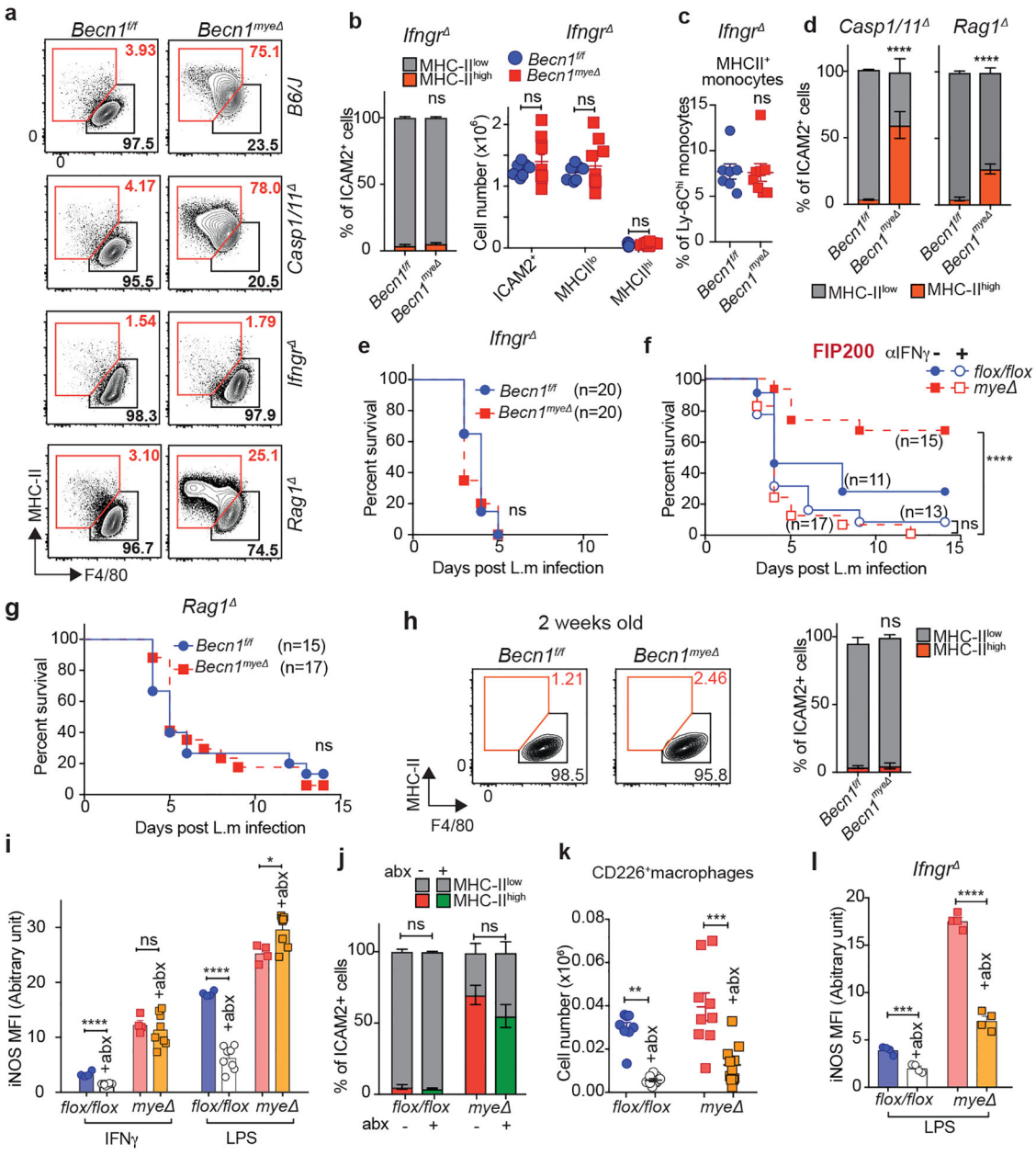

Figure 4. IFNγ signaling is necessary for macrophage activation and dominate effect over antibiotics-mediated immune quiescence in *Becn1* deficiency.

a, Flow cytometry plot of peritoneal macrophages obtained from naïve adult mice (Data represents 3 experiments, $n \geq 3$ mice each).

b, Peritoneal macrophages from naïve adult mice (*Becn1*$^{f/f}$*Ifngr*$^{\Delta}$, n=8; *Becn1*^{myeΔ}*Ifngr*$^{\Delta}$, n=9 mice; mean ± SEM, not significant by 2way ANOVA Sidak's multiple comparisons). **c**, Percentage of MHCII^{+} blood monocytes in naïve adult mice (*Becn1*$^{f/f}$*Ifngr*$^{\Delta}$, n=8; *Becn1*^{myeΔ}*Ifngr*$^{\Delta}$, n=9 mice; mean ± SEM, not significant by 2-tailed Mann-Whitney test).

d, Percent of MHC-II^{+}ICAM2^{+} peritoneal macrophages (*Becn1*$^{f/f}$*Casp1/11*$^{\Delta}$, n=6; *Becn1*^{myeΔ}*Casp1/11*$^{\Delta}$, n=6; *Becn1*$^{f/f}$*Rag1*$^{\Delta}$, n=7; *Becn1*^{myeΔ}*Rag1*$^{\Delta}$, n=8 mice, mean ± SEM, P by 2way ANOVA Sidak's multiple comparisons test).

e, **f**, **g**, Survival of mice after i.p. inoculation with 4~5×10^5 CFUs of *L. monocytogenes*. (Data pooled from 3 experiments. *P* by Log-rank Mantel-Cox test).

h, Flow cytometry analysis of peritoneal macrophages obtained from naïve neonatal mice (*Becn1*$^{f/f}$, *n*=5; *Becn1*^{myeΔ}, *n*=5 mice; mean ± SEM, not significant by 2way ANOVA Sidak's multiple comparisons on MHC-II^{high}).

i, **l**, Intracellular iNOS of *ex vivo* stimulated peritoneal macrophages (3 independent experiments, *Becn1*$^{f/f}$(Kool-Aid), *n*=4; *Becn1*$^{f/f}$(abx), *n*=8; *Becn1*^{myeΔ}(Kool-Aid), *n*=12; *Becn1*^{myeΔ}(abx), *n*=8; *n*=4 for all groups in (**I**); mean ± SEM, *P* by two-tailed t test).

j, Bar graph showing the fractions of ICAM2$^+$ macrophages (data pooled from ≥3 experiments, *Becn1*$^{f/f}$(Kool-Aid), *n*=14; *Becn1*$^{f/f}$(abx), *n*=17; *Becn1*^{myeΔ}(Kool-Aid), *n*=14; *Becn1*^{myeΔ}(abx), *n*=15; P_{adj} by 2way ANOVA Tukey's multiple comparisons on MHC-II^{high}). **k**, Quantification of CD226$^+$MHC-II$^+$ICAM2$^-$ macrophages (SPM) (data pooled from ≥3 experiments, *Becn1*$^{f/f}$(Kool-Aid), *n*=7; *Becn1*$^{f/f}$(abx), *n*=9; *Becn1*^{myeΔ}(Kool-Aid), *n*=9; *Becn1*^{myeΔ}(abx), *n*=10; P_{adj} by 2way ANOVA Sidak's multiple comparisons).